Truncated proposals for scalable and hassle-free simulation-based inference

Michael Deistler
University of Tübingen
michael.deistler@uni-tuebingen.de

Pedro J Gonçalves[*]
University of Tübingen
pedro.goncalves@uni-tuebingen.de

Jakob H Macke[*]
University of Tübingen
Max Planck Institute for Intelligent Systems
jakob.macke@uni-tuebingen.de

Abstract

Simulation-based inference (SBI) solves statistical inverse problems by repeatedly running a stochastic simulator and inferring posterior distributions from model-simulations. To improve simulation efficiency, several inference methods take a sequential approach and iteratively adapt the proposal distributions from which model simulations are generated. However, many of these sequential methods are difficult to use in practice, both because the resulting optimisation problems can be challenging and efficient diagnostic tools are lacking. To overcome these issues, we present Truncated Sequential Neural Posterior Estimation (TSNPE). TSNPE performs sequential inference with truncated proposals, sidestepping the optimisation issues of alternative approaches. In addition, TSNPE allows to efficiently perform coverage tests that can scale to complex models with many parameters. We demonstrate that TSNPE performs on par with previous methods on established benchmark tasks. We then apply TSNPE to two challenging problems from neuroscience and show that TSNPE can successfully obtain the posterior distributions, whereas previous methods fail. Overall, our results demonstrate that TSNPE is an efficient, accurate, and robust inference method that can scale to challenging scientific models.

1 Introduction

Computational models are an important tool to understand physical processes underlying empirically observed phenomena. These models, often implemented as numerical *simulators*, incorporate mechanistic knowledge about the physical process underlying data generation, and thereby provide an interpretable model of empirical observations. In many cases, several parameters of the simulator have to be inferred from data, e.g., with Bayesian inference. However, performing Bayesian inference in these models can be difficult: Running the simulator may be computationally expensive, evaluating the likelihood-function might be computationally infeasible, and the model might not be differentiable. In order to overcome these limitations, Approximate Bayesian Computation (ABC) methods [Beaumont et al., 2002, 2009], synthetic likelihood approaches [Wood, 2010], and neural network-based methods [e.g., Papamakarios and Murray, 2016, Hermans et al., 2020, Thomas et al., 2022] have been developed.

---

[*]Equal contribution

A subset of neural network-based methods, known as neural posterior estimation (NPE) [Papamakarios and Murray, 2016, Lueckmann et al., 2017, Greenberg et al., 2019], train a neural density estimator on simulated data such that the density estimator directly approximates the posterior. Unlike other methods, NPE does not require any further Markov-chain Monte-Carlo (MCMC) or variational inference (VI) steps. As it provides an *amortized* approximation of the posterior, which can be used to quickly evaluate and sample the approximate posterior for any observation, NPE allows the application in time-critical and high-throughput inference scenarios [Gonçalves et al., 2020, Radev et al., 2020, Dax et al., 2021], and fast application of diagnostic methods which require posterior samples for many different observations [Cook et al., 2006, Talts et al., 2018]. In addition, unlike methods targeting the likelihood (e.g., neural likelihood estimation, NLE [Papamakarios et al., 2019, Lueckmann et al., 2019]), NPE can learn summary statistics from data and it can use equivariances in the simulations to improve the quality of inference [Dax et al., 2021, 2022].

Figure 1: **APT vs TSNPE.** Top: Prior (gray) and true posterior (black). APT matches true posterior within the prior bounds but 'leaks' into region without prior support. TSNPE (ours) matches true posterior.

If inference is performed for a particular observation $\mathbf{x}_o$, sampling efficiency of NPE can be improved with *sequential* training schemes: Instead of drawing parameters from the prior distribution, they are drawn adaptively from a proposal (e.g., a posterior estimate obtained with NPE) in order to optimize the posterior accuracy for a particular $\mathbf{x}_o$. These procedures are called Sequential Neural Posterior Estimation (SNPE) [Papamakarios and Murray, 2016, Lueckmann et al., 2017, Greenberg et al., 2019] and have been reported to be more simulation-efficient than training the neural network only on parameters sampled from the prior, across a set of benchmark tasks [Lueckmann et al., 2021].

Despite the potential to improve simulation-efficiency, two limitations have impeded a more widespread adoption of SNPE by practitioners: First, the sequential scheme of SNPE can be unstable. SNPE requires a modification of the loss function compared to NPE, which suffers from issues that can limit its effectiveness on (or even prevent their application to) complex problems (see Sec. 2). Second, several commonly used diagnostic tools for SBI [Talts et al., 2018, Miller et al., 2021, Hermans et al., 2021] rely on performing inference across multiple observations. In SNPE (in contrast to NPE), this requires generating new simulations and network retraining for each observation, which often prohibits the use of such diagnostic tools [Lueckmann et al., 2021, Hermans et al., 2021].

Here, we introduce Truncated Sequential Neural Posterior Estimation (TSNPE) to overcome these limitations. TSNPE follows the SNPE formalism, but uses a proposal which is a *truncated* version of the prior: TSNPE draws simulations from the prior, but rejects them *before simulation* if they lie outside of the support of the approximate posterior. Thus, the proposal is (within its support) proportional to the prior, which allows us to train the neural network with maximum-likelihood in every round and, therefore, sidesteps the instabilities (and hence 'hassle') of previous SNPE methods. Our use of truncated proposals is strongly inspired by Blum and François [2010] and Miller et al. [2020, 2021], who proposed truncated proposals respectively for regression-adjustment approaches in ABC and for neural ratio estimation (see Discussion). Unlike methods based on likelihood(-ratio)-estimation [Miller et al., 2021, Hermans et al., 2021], TSNPE allows direct sampling and density evaluation of the approximate posterior, and thus permits computing expected coverage of the full posterior quickly (without MCMC) and at every iteration of the algorithm, thus allowing to diagnose failures of the method even for high-dimensional parameter spaces (we term this 'simulation-based coverage calibration' (SBCC), given its close connection with simulation-based calibration, SBC, Cook et al. [2006], Talts et al. [2018]).

We show that TSNPE is as efficient as the SNPE method 'Automatic Posterior Transformation' (APT, Greenberg et al. [2019]) on several established benchmark problems (Sec. 4.1). We then demonstrate that for two challenging neuroscience problems, TSNPE—but not APT—can robustly identify the posterior distributions (Sec. 4.2).
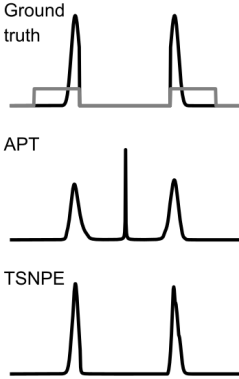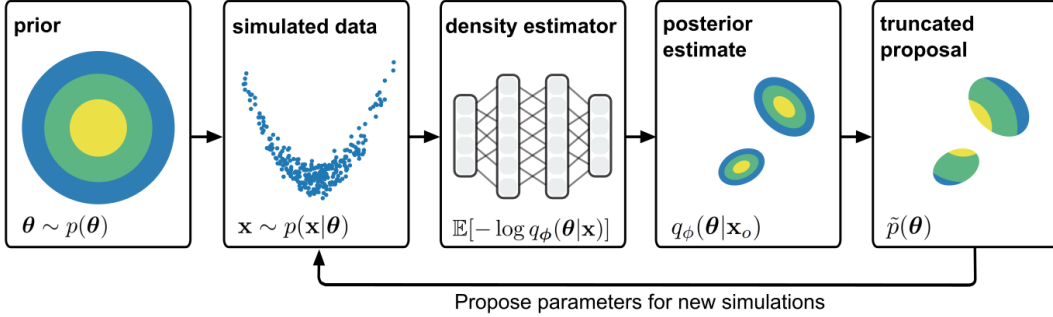
Figure 2: **Truncated Sequential Neural Posterior Estimation (TSNPE).** The method starts by sampling from the prior, running the simulator, and training a neural density estimator with maximum-likelihood to approximate the posterior. In subsequent rounds, parameters are sampled from the prior, but rejected if they lie outside of the support of the approximate posterior. With these proposals, the neural density estimator can be trained with maximum-likelihood in all rounds.

2 Background

In Neural Posterior Estimation (NPE), parameters are sampled from the prior $p(\boldsymbol{\theta})$ and simulated (i.e., $\mathbf{x}$ is sampled from $p(\mathbf{x}|\boldsymbol{\theta})$). Then, a neural density estimator $q_\phi(\boldsymbol{\theta}|\mathbf{x})$ (in our case a normalizing flow), with learnable parameters ϕ, is trained to minimize the loss:

$$\min_\phi \mathcal{L} = \min_\phi \mathbb{E}_{\boldsymbol{\theta}\sim p(\boldsymbol{\theta})} \mathbb{E}_{\mathbf{x}\sim p(\mathbf{x}|\boldsymbol{\theta})}[-\log q_\phi(\boldsymbol{\theta}|\mathbf{x})],$$

which is minimized if and only if, for a sufficiently expressive density estimator, $q_\phi(\boldsymbol{\theta}|\mathbf{x}) = p(\boldsymbol{\theta}|\mathbf{x})$ for all $\mathbf{x} \in \mathrm{supp}(p(\mathbf{x}))$ [Paige and Wood, 2016, Papamakarios and Murray, 2016]. Throughout this study, we refer to training with this loss function as maximum-likelihood training, although the neural density estimator targets the posterior directly.

Sequential Neural Posterior Estimation (SNPE) aims to infer the posterior distribution $p(\boldsymbol{\theta}|\mathbf{x}_o)$ for a particular observation $\mathbf{x}_o$. SNPE initially performs NPE and, thereby, obtains an initial estimate of the posterior distribution. It then samples parameters from a proposal $\tilde{p}(\boldsymbol{\theta})$, which is often chosen to be the previously obtained estimate of the posterior $\tilde{p}(\boldsymbol{\theta}) = q_\phi(\boldsymbol{\theta}|\mathbf{x}_o)$, and retrains the neural density estimator [Papamakarios and Murray, 2016]. This procedure can be repeated for several rounds.

Importantly, if parameters $\boldsymbol{\theta}$ are sampled from the proposal $\tilde{p}(\boldsymbol{\theta})$ rather than from the prior $p(\boldsymbol{\theta})$, the estimator $q_\phi(\boldsymbol{\theta}|\mathbf{x})$ that minimizes the maximum-likelihood loss function no longer converges to the true posterior. If one used the maximum-likelihood loss on data sampled from $\tilde{p}(\boldsymbol{\theta})$, i.e., $\mathcal{L} = \mathbb{E}_{\boldsymbol{\theta}\sim\tilde{p}(\boldsymbol{\theta})} \mathbb{E}_{\mathbf{x}\sim p(\mathbf{x}|\boldsymbol{\theta})}[-\log q_\phi(\boldsymbol{\theta}|\mathbf{x})]$, then $\mathcal{L}$ would be minimized by $q_\phi(\boldsymbol{\theta}|\mathbf{x}) \propto p(\boldsymbol{\theta}|\mathbf{x})\frac{\tilde{p}(\boldsymbol{\theta})}{p(\boldsymbol{\theta})}$, which is not the true posterior. Multiple schemes have been developed to overcome this [Papamakarios and Murray, 2016, Lueckmann et al., 2017]. The most recent of these methods, Automatic Posterior Transformation (APT, or SNPE-C, in its atomic version) [Greenberg et al., 2019, Durkan et al., 2020] employs a loss that aims to classify the parameter set that generated a particular data point among other parameter sets (details in Appendix Sec. 6.5).

While APT has been reported to significantly outperform previous methods, several studies have also described cases in which the approach exhibits performance issues: Both the original APT paper [Greenberg et al., 2019] and Durkan et al. [2020] reported that APT can show 'leakage' of posterior mass outside of bounded priors. We demonstrate this issue on a simple 1-dimensional simulator with bounded prior (Fig. 1, Appendix Fig. 7). The posterior estimated by APT is only required to match the true posterior density *within the support of the prior* (details in Appendix Sec. 6.5). Thus, after five rounds of APT, while the approximate posterior matches the true posterior within the bounds of the prior, a substantial fraction of posterior mass lies in regions with zero prior probability. In simple models, approximate posterior samples that lie outside of the prior bounds can be efficiently rejected. However, in models with high numbers of parameters, the rejection rate can become so large that drawing posterior samples which lie inside of the prior bounds is prohibitive. For example, Glöckler et al. [2022] reported a rejection rate of more than 99.9999% in a model with 31 parameters, thus requiring approximately one minute to draw a single posterior sample from within the prior bounds.

Algorithm 1: TSNPE

Inputs: prior $p(\boldsymbol{\theta})$, observation $\mathbf{x}_o$, simulations per round N, number of rounds R, ϵ that defines
  the highest-probability region (HPR$_\epsilon$)
Outputs: Approximate posterior q_ϕ.
Initialize: Proposal $\tilde{p}(\boldsymbol{\theta}) = p(\boldsymbol{\theta})$, dataset $\mathcal{X} = \{\}$
for $r \in [1, ..., R]$ **do**
    for $i \in [1, ..., N]$ **do**
        $\boldsymbol{\theta}_i \sim \tilde{p}(\boldsymbol{\theta})$
        simulate $\mathbf{x}_i \sim p(\mathbf{x}|\boldsymbol{\theta}_i)$
        add $(\boldsymbol{\theta}_i, \mathbf{x}_i)$ to $\mathcal{X}$
    $\phi^* = \arg\min_\phi -\frac{1}{N} \sum_{(\boldsymbol{\theta}_i, \mathbf{x}_i) \in \mathcal{X}} \log q_\phi(\boldsymbol{\theta}_i|\mathbf{x}_i)$
    Compute expected coverage$(\tilde{p}(\boldsymbol{\theta}), q_\phi)$;   `// see Alg. 2`
    $\tilde{p}(\boldsymbol{\theta}) \propto p(\boldsymbol{\theta}) \cdot \mathbb{1}_{\boldsymbol{\theta} \in \text{HPR}_\epsilon}$;   `// see Alg. 3`

We overcome these limitations by using 'truncated' proposal distributions. This allows us to train with maximum-likelihood at every round, thereby sidestepping issues of previous SNPE methods.

3 Methodology

3.1 Truncated proposals for SNPE

Given a particular observation $\mathbf{x}_o$, we suggest to restrict the proposals $\tilde{p}(\boldsymbol{\theta})$ to be proportional to the prior $p(\boldsymbol{\theta})$ at least in the $1 - \epsilon$ highest-probability-region (HPR$_\epsilon$, the smallest region that contains $1 - \epsilon$ of the mass) of $p(\boldsymbol{\theta}|\mathbf{x}_o)$, i.e.

$$\tilde{p}(\boldsymbol{\theta}) \propto p(\boldsymbol{\theta}) \cdot \mathbb{1}_{\boldsymbol{\theta} \in \mathcal{M}}$$

with HPR$_\epsilon(p(\boldsymbol{\theta}|\mathbf{x}_o)) \subseteq \mathcal{M}$. Thus, $\tilde{p}(\boldsymbol{\theta})$ is a 'truncated' proposal. The key insight is that, when using such a proposal and $\epsilon = 0$, one can train $q_\phi(\boldsymbol{\theta}|\mathbf{x})$ with maximum likelihood:

$$\min_\phi \mathcal{L} = \min_\phi \mathbb{E}_{\boldsymbol{\theta} \sim \tilde{p}(\boldsymbol{\theta})} \mathbb{E}_{\mathbf{x} \sim p(\mathbf{x}|\boldsymbol{\theta})} [-\log q_\phi(\boldsymbol{\theta}|\mathbf{x})],$$

and $q_\phi(\boldsymbol{\theta}|\mathbf{x}_o)$ will still converge to $p(\boldsymbol{\theta}|\mathbf{x}_o)$ (Proof in Appendix Sec. 6.2).

We estimate $\mathcal{M}$ as the HPR$_\epsilon$ of the approximate posterior $\mathcal{M} = \text{HPR}_\epsilon(q_\phi(\boldsymbol{\theta}|\mathbf{x}_o))$. Since the maximum-likelihood loss employed to train $q_\phi(\boldsymbol{\theta}|\mathbf{x})$ is support-covering, the HPR$_\epsilon$ of $q_\phi(\boldsymbol{\theta}|\mathbf{x}_o)$ tends to cover the HPR$_\epsilon$ of $p(\boldsymbol{\theta}|\mathbf{x}_o)$ [Bishop and Nasrabadi, 2006].

In order to obtain the HPR$_\epsilon$ of $q_\phi(\boldsymbol{\theta}|\mathbf{x}_o)$, we define a threshold $\boldsymbol{\tau}$ on the approximate posterior density $q_\phi(\boldsymbol{\theta}|\mathbf{x}_o)$. To do so, we use a normalizing flow as $q_\phi(\boldsymbol{\theta}|\mathbf{x})$, which allows for closed-form density evaluation and fast sampling. We then approximate the HPR$_\epsilon$ of $q_\phi(\boldsymbol{\theta}|\mathbf{x}_o)$ as

$$\text{HPR}_\epsilon(q_\phi(\boldsymbol{\theta}|\mathbf{x}_o)) \approx \mathbb{1}_{q_\phi(\boldsymbol{\theta}|\mathbf{x}_o) > \boldsymbol{\tau}}.$$

We chose $\boldsymbol{\tau}$ as the ϵ-quantile of approximate posterior densities of samples from $q_\phi(\boldsymbol{\theta}|\mathbf{x}_o)$, and evaluated TSNPE for $\epsilon = 10^{-3}, 10^{-4}$, and 10^{-5}. Values of $\epsilon > 0$ yield a proposal prior which has smaller support than the current estimate of the posterior, e.g., using $\epsilon = 10^{-3}$ neglects 0.1% of mass from the approximate-posterior support. Thus, this approach leads to errors in posterior estimation, e.g., to 'under-covered' posteriors (Appendix Sec. 6.10). However, empirically, the error induced by this truncation is negligible, as we will demonstrate on several benchmark tasks. We note that TSNPE can be trained on data pooled from all rounds (Appendix Sec. 6.2). TSNPE is summarized in Alg. 1 (Fig. 2).

3.2 Sampling from the truncated proposal

To generate training data for subsequent rounds, we have to draw samples from the truncated proposal $\tilde{p}(\boldsymbol{\theta})$, and here we explored rejection sampling and sampling importance resampling (SIR) [Rubin, 1988]. For rejection sampling, we sample the prior $\boldsymbol{\theta} \sim p(\boldsymbol{\theta})$ and accept samples only if their probability under the approximate posterior $q_\phi(\boldsymbol{\theta}|\mathbf{x})$ is above threshold $\boldsymbol{\tau}$.
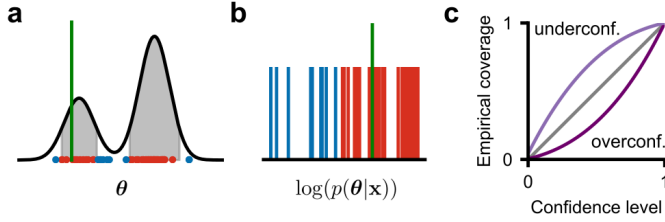
Figure 3: **Diagnostic tool.** (a) Parameter θ^* (green) lies within the 1-α confidence region (gray) of the estimated posterior. (b) $\log(p(\theta^*|x))$ is above the 1-α quantile of posterior samples. (c) 1-α versus empirical coverage, averaged over θ^*.

This strategy samples from the truncated proposal exactly, but can fail if the rejection rate becomes too high. To deal with these situations, we used SIR. For each sample from the truncated proposal, SIR draws K samples from the approximate posterior, computes weights $w_{i=1...K} = p(\theta_i)\mathbb{1}_{\theta_i \in \mathcal{M}}/q_\phi(\theta_i|\mathbf{x})$, normalizes w_i such that they sum to one, draws from a categorical distribution with weights $s \sim \text{Categorical}(w_i)$, and selects the posterior sample with index s. SIR requires a fixed sampling budget of K posterior samples per sample from the truncated proposal and returns exact samples from the truncated proposal for $K \to \infty$. Too low values of K lead to too narrow proposals and posterior approximations. When run for a number of rounds, this behaviour reinforces itself and can lead to divergence of TSNPE (Appendix Fig. 13). We, thus, chose a high value $K = 1024$. In our experiments, we did not observe poor SIR performance, but we emphasise the importance of using tools to diagnose potential failures of TSNPE (see below) or SIR (e.g. by inspecting the effective sample size, Appendix Sec. 6.12). When SIR fails, methods such as nested sampling, adaptive multi-level splitting, or sequential Monte-Carlo sampling could be viable alternatives [Skilling, 2004, Cérou and Guyader, 2007, Doucet et al., 2001]. We discuss computational costs of rejection sampling and SIR in Appendix Sec. 6.11.

3.3 Coverage diagnostic

In order for the estimated posterior $q_\phi(\theta|\mathbf{x}_o)$ to converge to $p(\theta|\mathbf{x}_o)$, TSNPE requires $\text{supp}(p(\theta|\mathbf{x}_o)) \subseteq \text{HPR}_\epsilon(q_\phi(\theta|\mathbf{x}_o))$, i.e., the estimated posterior must be broader than the true posterior (proof in Appendix Sec. 6.2). In order to diagnose whether the posterior is, on average, sufficiently broad, we perform expected coverage tests as proposed in Dalmasso et al. [2020], Miller et al. [2021], Hermans et al. [2021].

As described in Dalmasso et al. [2020], Rozet et al. [2021] and illustrated in Fig. 3, the coverage of the approximate posterior can be computed as

$$1 - \alpha = \int q_\phi(\theta|\mathbf{x}^*)\mathbb{1}(q_\phi(\theta^*|\mathbf{x}^*) \geq q_\phi(\theta|\mathbf{x}^*))d\theta$$

where θ^* is sampled from the truncated proposal and $\mathbf{x}^*$ is the corresponding simulator output. In order to approximate this integral, one has to either evaluate the approximate posterior on a grid [Dalmasso et al., 2020, Hermans et al., 2021] or apply a Monte-Carlo average which includes repeatedly sampling (and evaluating) the (unnormalized) approximate posterior [Miller et al., 2021, Rozet et al., 2021]. The first option does not scale to high-dimensional spaces whereas the second is computationally expensive for methods estimating likelihood(-ratios) and, thus, require MCMC. In contrast, the TSNPE-posterior can be sampled from and evaluated in closed-form, leading to a computationally efficient and scalable diagnostic which can be run after every training round.

Expected coverage can be computed as an average of the coverage across multiple pairs $(\theta^*, \mathbf{x}^*)$ [Miller et al., 2021, Hermans et al., 2021] and should match the confidence level for all confidence levels $(1 - \alpha) \in [0, 1]$ (Fig. 3c). We term this procedure of computing the empirical coverage 'simulation-based coverage calibration' (SBCC), due to its close connection with SBC [Cook et al., 2006, Talts et al., 2018] (identical under certain conditions, Appendix Sec. 6.6). For TSNPE, it is important that the empirical expected coverage matches the confidence level for high confidence levels (i.e., for small α), since overconfidence in these regions would indicate that ground-truth parameters θ^* are falsely excluded from the $\text{HPR}_{\epsilon=\alpha}$. SBCC is summarized in Appendix Alg. 2.
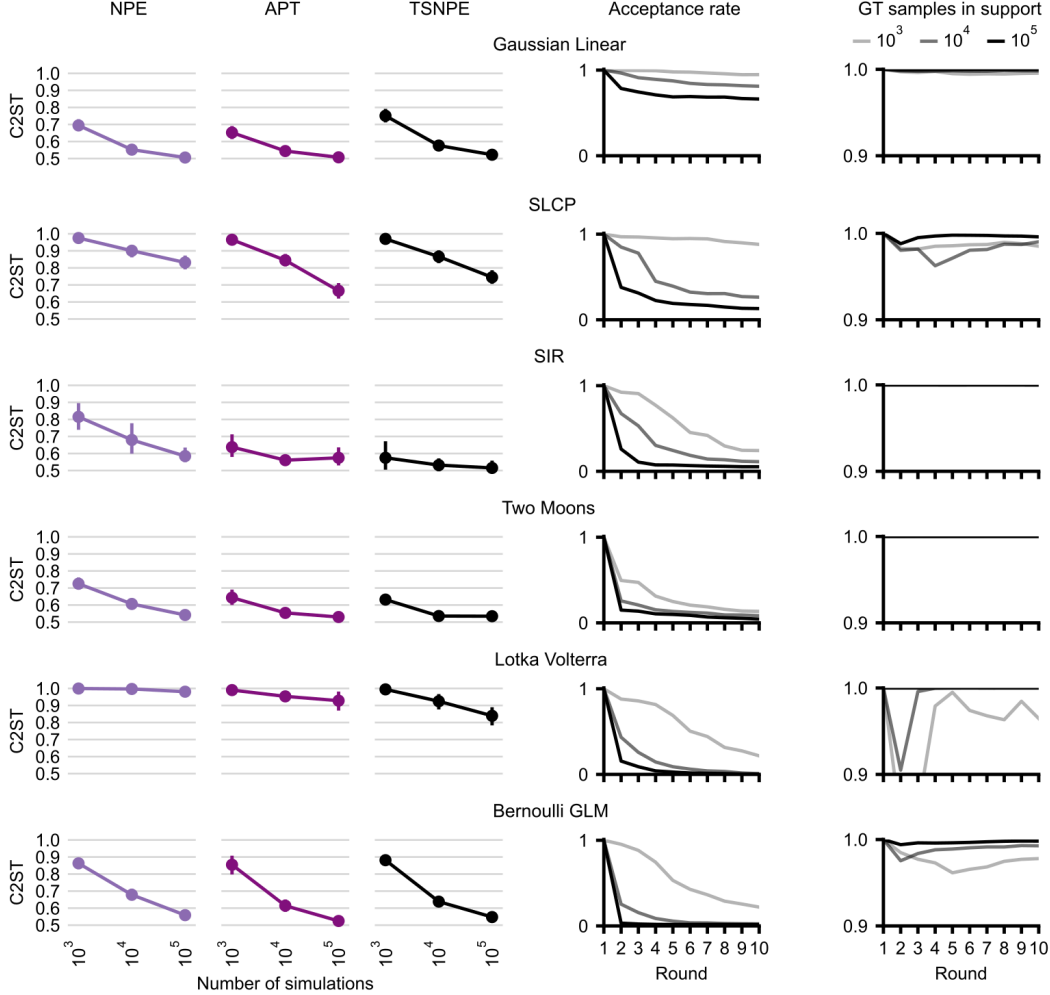
5

Figure 4: **Performance on six benchmark tasks.** Left three columns: classifier two-sample test accuracy (C2ST) of NPE (left), APT (middle), and TSNPE (right) for three simulation budgets. Forth column: Fraction of prior samples within the approximate-posterior HPR_ϵ in each round for each simulation budget. Fifth column: Fraction of true-posterior samples within the approximate-posterior HPR_ϵ. TSNPE with $\epsilon = 10^{-4}$ and rejection sampling from truncated proposal.

4 Results

We evaluated TSNPE on several benchmark tasks and on two complex problems from neuroscience. We found that TSNPE performs as well as APT on the benchmark tasks and that it is robust to choices of ϵ. In addition, we found that, in contrast with APT, TSNPE can successfully infer the posterior distribution for complex models with large numbers of parameters.

4.1 Performance on benchmark tasks

We compared TSNPE with NPE and APT on six benchmark tasks for which samples from the ground-truth posterior are available (see Appendix Sec. 6.9 for tasks) [Lueckmann et al., 2021]. We quantified the performance with a classifier two-sample test (C2ST), for which 0.5 indicates that the approximate posterior is identical to the ground-truth posterior, whereas 1.0 implies that the distributions can be completely separated by a classifier. Overall, APT and TSNPE perform similarly well and both outperform NPE (Fig. 4, left three columns). On two of the six tasks (Gaussian Linear and SLCP), APT has slightly better performance than TSNPE, whereas on two other tasks (SIR
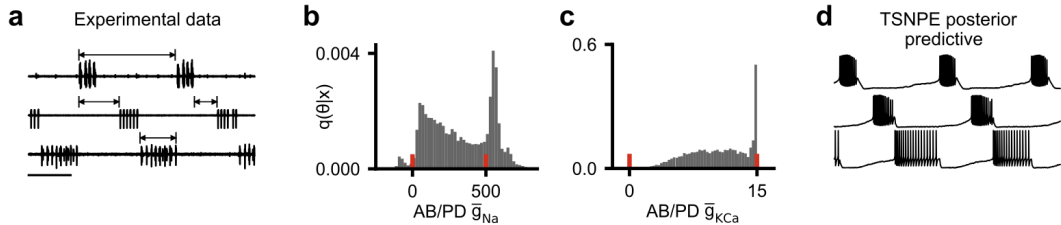
Figure 5: **Pyloric network inference.** (a) Data [Haddad and Marder, 2021]. (b) APT approximate posterior (1D-marginal) exhibits leakage (red: prior bounds). (c) APT approximate posterior when forcing the density estimator into constrained space. The spike at the upper prior bound is at odds with previously published posterior distributions [Gonçalves et al., 2020, Deistler et al., 2021, Glöckler et al., 2022] and produces poor predictive samples (Appendix Fig. 19). (d) TSNPE posterior predictive sample matches summary statistics of the experimental data.

and Lotka-Volterra), TSNPE outperforms APT. Overall, TSNPE and APT perform similarly well, demonstrating that TSNPE is competitive with previous methods on benchmark tasks.

In order to get insights into the improved performance of TSNPE as compared to NPE, we computed the fraction of prior samples that lie within the HPR_ϵ of the approximate posterior (Fig. 4, fourth column). In tasks with broad posteriors and few simulations, the HPR_ϵ is almost as wide as the prior and thus the performances of NPE and TSNPE are similar (e.g., SLCP with 1k simulations). In other tasks and with more simulations, the HPR_ϵ is much narrower than the prior, leading to an improvement in simulation efficiency (e.g., Lotka-Volterra with 100k simulations).

Finally, we evaluated whether the HPR_ϵ of the approximate posterior contains the support of the true posterior (Fig. 4, fifth column). We computed the fraction of true-posterior samples within the HPR_ϵ of the approximate posterior. For most tasks, fewer than 0.1% of samples were excluded, and the rate of erroneously rejected samples decreased as more simulations were used. In the Lotka-Volterra task with 1k and 10k simulations, many ground-truth samples were rejected and TSNPE performed poorly, but NPE and APT also failed to solve the task. Thus, while truncated proposals can potentially induce posterior biases, these only have a negligible effect on the performance of TSNPE. We note that TSNPE performance is qualitatively unaffected by the choice of $\epsilon \leq 10^{-4}$ and proposal sampling scheme (Appendix Fig. 8, Fig. 9, Fig.10). Applying truncated proposals to APT leads to equally good or worse performance than 'standard' APT, depending on the task (Appendix Fig. 14).

4.2 Efficient and robust inference in two complex neuroscience problems

Next, we evaluate the performance of TSNPE on two challenging neuroscience problems, where the competitive advantage of TSNPE is fully realized.

Pyloric network   We applied TSNPE to a challenging real-world simulator from neuroscience: The pyloric network of the stomatogastric ganglion in the crab *Cancer Borealis* [Prinz et al., 2003, 2004]. The model has 31 parameters and simulates 3 voltage traces that we reduce to 18 summary statistics. The prior distribution is uniform within previously described parameter ranges [Prinz et al., 2004, Gonçalves et al., 2020]. We identify the posterior distribution given experimentally observed data [Haddad and Marder, 2021] (Fig. 5a) with APT and TSNPE (13 rounds, 30k simulations per round).

When applying APT 'out of the box' (from 'sbi' toolbox [Tejero-Cantero et al., 2020]), the rate of approximate-posterior samples within the prior bounds was 0.02% after the second round and 0.0000% after the third round (Fig. 5b), which rendered a fourth round too computationally expensive.

We attempted to overcome these issues by appending a transformation T to the density estimator $q_\phi(\boldsymbol{\theta}|\mathbf{x})$ such that its support is constrained to match the support of the prior. In practice, we used a sigmoid transformation. While the resulting approximate posterior exhibited no leakage, this setup revealed another problem when running APT: In transformed (i.e., unbounded) space, the density estimator $q_\phi(\boldsymbol{\theta}|\mathbf{x})$ can put significant mass in regions outside of the training data. When forced into constrained space, these 'leaking' regions lead to spikes at the bounds of the parameter space (Fig. 5c, further details in Appendix Sec. 6.5; illustration, additional tests and full posterior in Appendix
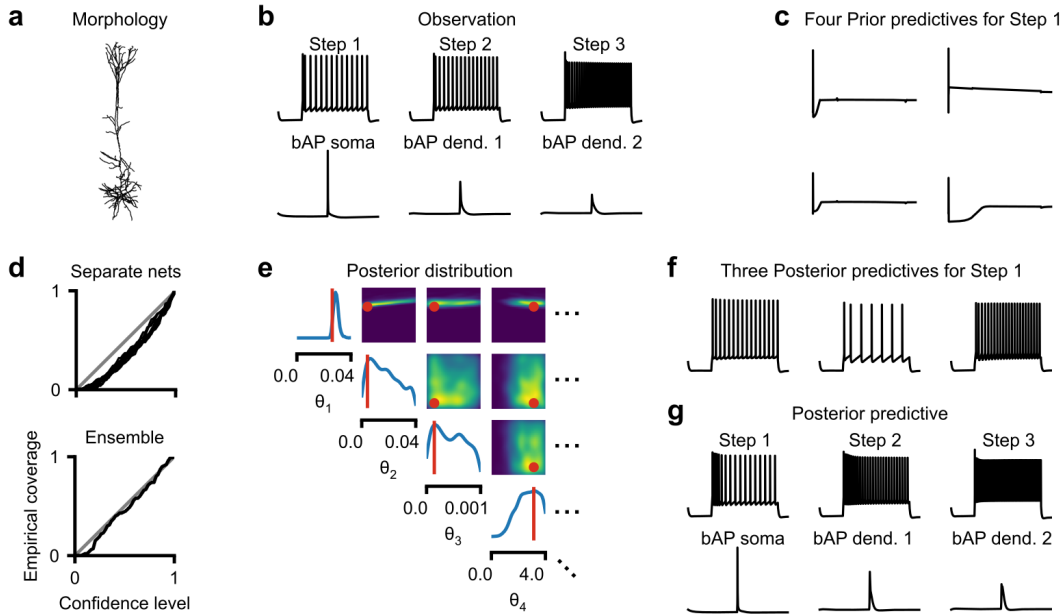
Figure 6: **TSNPE on L5PC.** (a) Cell morphology. (b) Observation. (c) Four prior samples for the Step 1 protocol. (d) Coverage for 1 and 10 neural nets. (e) Posterior. True parameter in red. (f) Three posterior predictives for the Step 1 protocol. (g) One posterior predictive for all protocols.

Figs. 17, 16 and 18). These spikes are at odds with previously published posterior distributions [Gonçalves et al., 2020, Deistler et al., 2021, Glöckler et al., 2022] and samples from these parameter regions do not produce good simulations (Appendix Fig. 19). This demonstrates that leakage occurs in APT even when the density estimator is forced into constrained space and that these issues lead to an incorrect posterior approximation as well as to poor predictive samples.

We applied TSNPE to this task for 13 rounds without any issue. The resulting posterior produces samples that closely match the observed data (Fig. 5d, more samples in Appendix Fig. 15, posterior distribution across all 31 parameters in Appendix Fig. 20). The obtained posterior is similar to previously published posteriors [Gonçalves et al., 2020, Deistler et al., 2021, Glöckler et al., 2022].

Multicompartment model of a single neuron   Finally, we turn to a landmark problem in neuroscience for which the posterior has not yet been identified: A morphologically detailed model of a thick-tufted layer 5 pyramidal cell (L5PC) from the neocortex [Ramaswamy et al., 2015, Markram et al., 2015, Van Geit et al., 2016]. The model describes the response of a neuron to current stimuli of different strengths. The model has approximately 7000 separate compartments which compose the anatomy of the cell (Fig. 6a). Each compartment has dynamics based on the Hodgkin-Huxley equations [Hodgkin and Huxley, 1952] and contains multiple ion channels (details in Van Geit et al. [2016]). The model has 20 free parameters which are the maximal channel conductances and time constants of the ion channels. The simulation consists of four separate simulations corresponding to experimental protocols which describe the voltage response to different stimuli. For the first three protocols (Step 1, Step 2, Step 3), each voltage response is characterized by 10 summary statistics. The fourth protocol models the back-propagation of the voltage response through the dendritic tree and is captured by 5 additional summary statistics (bAP soma, bAP dend. 1, bAP dend. 2). In total, the model produces 35 summary statistics, to which we add Gaussian noise with diagonal covariance matrix capturing the response variability of previously reported measurements [Hay et al., 2011].

Our goal is to infer the posterior distribution over 20 parameters given 35 summary statistics that were simulated—and thus have a known ground-truth parameter set— to resemble experimentally observed activity (Fig. 6b). The prior is a uniform distribution within previously established bounds [Van Geit et al., 2016]. A major difficulty in fitting this model is that a large fraction of prior samples generate summary statistics that are very different from the observed data: In particular, about 99.98% of prior predictives contain at least one summary statistic that is undefined, e.g., time to first spike is

8

undefined in the absence of spikes (Fig. 6c). When a summary statistic is undefined, we assign it a value that is substantially outside the range of the observed data (Appendix Sec. 6.14).

We ran TSNPE over six rounds (hyperparameters in Appendix Sec. 6.15). In each round, we ran 30k simulations, leading to a total of 180k simulations. After every round, we evaluated the expected coverage with SBCC. After the first round, the approximate posterior exhibited poor expected coverage (Fig. 6d top). Therefore, as suggested by Hermans et al. [2021], we used an ensemble of 10 neural density estimators to ensure that the approximate posterior is sufficiently broad (Fig. 6d bottom). Although the approximate posterior remains underconfident, the empirical expected coverage closely matches the confidence level for high-confidence levels, which is crucial for TSNPE (Sec. 3.3).

The TSNPE-posterior has several parameters with broad marginals, demonstrating that this model exhibits 'degeneracy', a widespread phenomenon in biological systems [Marder and Taylor, 2011] (Fig. 6e, Appendix Sec. 6.14 for parameter names). Other marginals are narrow, demonstrating that the model is sensitive to changes in these parameters. Posterior predictive samples closely match the observed data (Fig. 6f,g; more samples in Appendix Fig. 22). We emphasize that fitting such morphologically-detailed neuron models is a challenging and widespread problem in neuroscience, one for which commonly used methods [e.g., genetic algorithms, Druckmann et al., 2007, Van Geit et al., 2016] are often simulation-inefficient or do not estimate the full posterior distribution. We show promising results, suggesting that TSNPE could be applied to other complex single-neuron models.

In contrast, with 'out of the box' APT, none of the 10M approximate-posterior samples was within the prior bounds after the second round. This rendered a third round too computationally expensive. Overall, the results on the pyloric network model and on the multicompartment model demonstrate that TSNPE is an efficient and robust method that scales to complex and high-dimensional models that were inaccessible to the state-of-the-art method APT.

5   Discussion

We presented a new method to perform Bayesian inference in implicit models, which we call Truncated Sequential Neural Posterior Estimation (TSNPE). Like previous methods, TSNPE adaptively selects parameters to improve simulation-efficiency and allow posterior inference in complex models with many parameters. The key ingredient is that TSNPE samples parameters from a 'truncated' region of the prior, and thus overcomes instabilities of previous methods while maintaining simulation efficiency. In order to diagnose potential errors of TSNPE, we developed a coverage test that can be run quickly and at every round of TSNPE. TSNPE presents a new variant of SNPE which is at least as powerful as previous variants on benchmark tasks, but provides a powerful alternative which is able to solve inference problems on which the state-of-the-art method APT failed.

Related work   TSNPE differs from automatic posterior transformation (APT, SNPE-C) in its proposal and its loss function: TSNPE uses a truncated prior as proposal, while APT can flexibly use any proposal, which, e.g., allows for more sophisticated active learning rules [Lueckmann et al., 2019, Järvenpää et al., 2019]. However, APT's flexibility requires a modification of NPE loss function, which can be an impediment to its usage in practice: First, the modification can lead to 'leakage', which can make it prohibitive to draw samples within prior bounds. Second, APT loss requires an explicit prior and thus, cannot be applied to models in which the prior can only be sampled [Ramesh et al., 2022]. Third, current formulations of APT cannot discard parameters leading to invalid simulations as the posterior mass would 'leak' into parameter regions which only produce invalid simulations (Appendix Sec. 6.5). It might be possible that these issues are resolved using a modified formulation of APT, e.g., by combining its atomic loss with additional loss terms, or preventing leakage by penalizing 'bad' parameters [Greenberg et al., 2019]. In cases in which leakage prevents application of APT (in particular, in high-dimensional problems), TSNPE provides an alternative.

Our method is inspired by previous work that introduced a mechanism to post-hoc correct samples obtained by an Approximate Bayesian Computation (ABC) algorithm [Blum and François, 2010], i.e., 'regression adjustment ABC'. Their method draws samples from a truncated region of the prior to avoid correction terms, but estimates the posterior density with ABC samples—rather than using a flexible neural density estimator—and estimates the support by training a dedicated support-vector machine. In addition, the method runs a single round of truncation and retraining, whereas we demonstrate that TSNPE can be robustly applied across 10 rounds.

Truncated proposals have also been proposed for neural ratio estimation [Truncated Marginal Neural Ratio Estimation (TMNRE) Miller et al., 2021]: TMNRE uses truncated proposals to efficiently infer selected posterior marginals while being amortised around the observation, allowing to test the coverage properties of the selected marginals, e.g., with SBC [Cook et al., 2006, Talts et al., 2018]. In addition, truncating based on the marginals allows TMRNE to sample from the truncated proposal without rejection or SIR sampling. In contrast, TSNPE aims at efficiently inferring the full posterior distribution by proposals that avoid the correction of SNPE loss function. Truncating the proposal based on the full posterior rather than on the marginals can lead to drastically narrower proposals: E.g., on the pyloric network problem, truncation based on posterior marginals rejects 20% of prior samples versus 99.94% rejection based on the posterior joint. In addition, while TMNRE uses the expected coverage to test the consistency of the posterior marginals, TSNPE can test the expected coverage of the full posterior distribution.

Possible failure modes   The main failure mode of TSNPE will occur if the truncated proposal excludes significant portions of density mass of the true posterior (e.g., if the estimate misses posterior modes). In these cases, the learned approximate posterior will put systematically too little mass in the excluded regions. We recommend the use of diagnostic tools such as SBCC to identify such failures [Cook et al., 2006, Miller et al., 2021, Hermans et al., 2021, Rozet et al., 2021].

In addition, if the true posterior has unbounded support, any finite values of $\epsilon > 0$ will lead to a biased approximate posterior which puts too little weight in the posterior tails. In that case, and when running TSNPE across many rounds, the errors from each individual round could accumulate. Although we did not observe this bias to significantly affect the algorithm performance on several benchmark tasks, we cannot exclude the possibility of a substantial performance degradation when running TSNPE for a larger number of rounds ($\gg$10).

Finally, unlike SNPE methods that use the previous estimate of the posterior as the proposal distribution, our method requires a scheme to sample from a truncated proposal. If the sampling scheme is inaccurate (i.e., if it does not produce a proposal distribution that is proportional to the prior within the truncated region), the results of TSNPE will be biased. To avoid this, we recommend using rejection sampling by default and using SIR or sequential Monte-Carlo methods only if rejection sampling is too computationally expensive. For SIR, it is important to use a large oversampling factor K (e.g., $K = 1024$) and use diagnostic tools such as effective sample size (Appendix Sec. 6.12, Fig. 13).

Simulation-based coverage calibration   In order to diagnose whether the approximate posterior is broader than the true posterior, we applied SBCC, a coverage test for TSNPE [Cook et al., 2006, Rozet et al., 2021]. SBCC evaluates the expected coverage of the approximate posterior without evaluating it on a grid [Dalmasso et al., 2020, Hermans et al., 2021] and, unlike diagnostic tools for methods based on learning the likelihood(-ratio), does not require MCMC runs for multiple observations $\mathbf{x}$ [Miller et al., 2021]. This allows SBCC to be run quickly and for models with many parameters. In addition, in contrast to diagnostic tools for likelihood-free inference with Approximate Bayesian Computation, SBCC does not require an additional step to estimate the density of approximate posterior samples [Prangle et al., 2014]. We note that, since SBCC is a variation of SBC [Cook et al., 2006, Talts et al., 2018], it only ensures that the HPR$_\epsilon$ is correct *on average* across observations, not for a particular observation. In principle, SBCC could be applied to other SNPE variants, although empirically the impact of arbitrary proposals on SBCC performance is currently unclear.

Conclusion   Overall, TSNPE combines the simulation-efficiency of sequential neural posterior estimation with the robustness and coverage-tests of non-sequential methods. We demonstrated that it allows to scale neural posterior estimation to complex and high-dimensional scientific problems.

Acknowledgments and Disclosure of Funding

References

M A Beaumont, J Cornuet, J Marin, and C P Robert. Adaptive approximate bayesian computation. *Biometrika*, 2009.

Mark A Beaumont, Wenyang Zhang, and David J Balding. Approximate bayesian computation in population genetics. *Genetics*, 162(4):2025–2035, 2002.

Christopher M Bishop and Nasser M Nasrabadi. *Pattern recognition and machine learning*, volume 4. Springer, 2006.

Michael GB Blum and Olivier François. Non-linear regression models for approximate bayesian computation. *Statistics and Computing*, 20(1):63–73, 2010.

Bob Carpenter, Andrew Gelman, Matthew D Hoffman, Daniel Lee, Ben Goodrich, Michael Betancourt, Marcus Brubaker, Jiqiang Guo, Peter Li, and Allen Riddell. Stan: A probabilistic programming language. *Journal of statistical software*, 76(1), 2017.

Frédéric Cérou and Arnaud Guyader. Adaptive multilevel splitting for rare event analysis. *Stochastic Analysis and Applications*, 25(2):417–443, 2007.

Samantha R Cook, Andrew Gelman, and Donald B Rubin. Validation of software for bayesian models using posterior quantiles. *Journal of Computational and Graphical Statistics*, 15(3):675–692, 2006.

Niccolò Dalmasso, Taylor Pospisil, Ann B Lee, Rafael Izbicki, Peter E Freeman, and Alex I Malz. Conditional density estimation tools in python and r with applications to photometric redshifts and likelihood-free cosmological inference. *Astronomy and Computing*, 30:100362, 2020.

Maximilian Dax, Stephen R Green, Jonathan Gair, Jakob H Macke, Alessandra Buonanno, and Bernhard Schölkopf. Real-time gravitational wave science with neural posterior estimation. *Physical review letters*, 127(24):241103, 2021.

Maximilian Dax, Stephen R Green, Jonathan Gair, Michael Deistler, Bernhard Schölkopf, and Jakob H. Macke. Group equivariant neural posterior estimation. In *International Conference on Learning Representations*, 2022.

Michael Deistler, Jakob H Macke, and Pedro J Gonçalves. Energy efficient network activity from disparate circuit parameters. *bioRxiv*, 2021.

Petar M Djuric, Jayesh H Kotecha, Jianqui Zhang, Yufei Huang, Tadesse Ghirmai, Mónica F Bugallo, and Joaquin Miguez. Particle filtering. *IEEE signal processing magazine*, 20(5):19–38, 2003.

Arnaud Doucet, Nando De Freitas, Neil James Gordon, et al. *Sequential Monte Carlo methods in practice*, volume 1. Springer, 2001.

Shaul Druckmann, Yoav Banitt, Albert A Gidon, Felix Schürmann, Henry Markram, and Idan Segev. A novel multiple objective optimization framework for constraining conductance-based neuron models by experimental data. *Frontiers in Neuroscience*, 1:1, 2007.

Conor Durkan, Artur Bekasov, Iain Murray, and George Papamakarios. Neural spline flows. *Advances in neural information processing systems*, 32, 2019.

Conor Durkan, Iain Murray, and George Papamakarios. On contrastive learning for likelihood-free inference. In *International Conference on Machine Learning*, pages 2771–2781. PMLR, 2020.

Manuel Glöckler, Michael Deistler, and Jakob H. Macke. Variational methods for simulation-based inference. In *International Conference on Learning Representations*, 2022.

Pedro J Gonçalves, Jan-Matthis Lueckmann, Michael Deistler, Marcel Nonnenmacher, Kaan Öcal, Giacomo Bassetto, Chaitanya Chintaluri, William F Podlaski, Sara A Haddad, Tim P Vogels, et al. Training deep neural density estimators to identify mechanistic models of neural dynamics. *Elife*, 9:e56261, 2020.

David Greenberg, Marcel Nonnenmacher, and Jakob Macke. Automatic posterior transformation for likelihood-free inference. In *International Conference on Machine Learning*, pages 2404–2414. PMLR, 2019.

Sara Ann Haddad and Eve Marder. Recordings from the c. borealis stomatogastric nervous system at different temperatures in the decentralized condition. *URL https://doi.org/10.5281/zenodo*, 5139650, 2021.

Etay Hay, Sean Hill, Felix Schürmann, Henry Markram, and Idan Segev. Models of neocortical layer 5b pyramidal cells capturing a wide range of dendritic and perisomatic active properties. *PLoS computational biology*, 7(7):e1002107, 2011.

Joeri Hermans, Volodimir Begy, and Gilles Louppe. Likelihood-free mcmc with amortized approximate ratio estimators. In *International Conference on Machine Learning*, pages 4239–4248. PMLR, 2020.

Joeri Hermans, Arnaud Delaunoy, François Rozet, Antoine Wehenkel, and Gilles Louppe. Averting a crisis in simulation-based inference. *arXiv preprint arXiv:2110.06581*, 2021.

Alan L Hodgkin and Andrew F Huxley. A quantitative description of membrane current and its application to conduction and excitation in nerve. *The Journal of physiology*, 117(4):500, 1952.

Marko Järvenpää, Michael U Gutmann, Arijus Pleska, Aki Vehtari, and Pekka Marttinen. Efficient acquisition rules for model-based approximate bayesian computation. *Bayesian Analysis*, 14(2): 595–622, 2019.

William Ogilvy Kermack and Anderson G McKendrick. A contribution to the mathematical theory of epidemics. *Proceedings of the royal society of london. Series A, Containing papers of a mathematical and physical character*, 115(772):700–721, 1927.

Augustine Kong. A note on importance sampling using standardized weights. *University of Chicago, Dept. of Statistics, Tech. Rep*, 348, 1992.

Jan-Matthis Lueckmann, Pedro J Goncalves, Giacomo Bassetto, Kaan Öcal, Marcel Nonnenmacher, and Jakob H Macke. Flexible statistical inference for mechanistic models of neural dynamics. *Advances in neural information processing systems*, 30, 2017.

Jan-Matthis Lueckmann, Giacomo Bassetto, Theofanis Karaletsos, and Jakob H Macke. Likelihood-free inference with emulator networks. In *Symposium on Advances in Approximate Bayesian Inference*, pages 32–53. PMLR, 2019.

Jan-Matthis Lueckmann, Jan Boelts, David Greenberg, Pedro Goncalves, and Jakob Macke. Benchmarking simulation-based inference. In *International Conference on Artificial Intelligence and Statistics*, pages 343–351. PMLR, 2021.

Eve Marder and Adam L Taylor. Multiple models to capture the variability in biological neurons and networks. *Nature neuroscience*, 14(2):133–138, 2011.

Henry Markram, Eilif Muller, Srikanth Ramaswamy, Michael W Reimann, Marwan Abdellah, Carlos Aguado Sanchez, Anastasia Ailamaki, Lidia Alonso-Nanclares, Nicolas Antille, Selim Arsever, et al. Reconstruction and simulation of neocortical microcircuitry. *Cell*, 163(2):456–492, 2015.

Luca Martino, Víctor Elvira, and Francisco Louzada. Effective sample size for importance sampling based on discrepancy measures. *Signal Processing*, 131:386–401, 2017.

Benjamin Miller, Alex Cole, Patrick Forré, Gilles Louppe, and Christoph Weniger. Truncated marginal neural ratio estimation. *Advances in Neural Information Processing Systems*, 34, 2021.

Benjamin Kurt Miller, Alex Cole, Gilles Louppe, and Christoph Weniger. Simulation-efficient marginal posterior estimation with swyft: stop wasting your precious time. *arXiv preprint arXiv:2011.13951*, 2020.

Brooks Paige and Frank Wood. Inference networks for sequential monte carlo in graphical models. In *International Conference on Machine Learning*, pages 3040–3049. PMLR, 2016.

George Papamakarios and Iain Murray. Fast ε-free inference of simulation models with bayesian conditional density estimation. *Advances in neural information processing systems*, 29, 2016.

George Papamakarios, David Sterratt, and Iain Murray. Sequential neural likelihood: Fast likelihood-free inference with autoregressive flows. In *The 22nd International Conference on Artificial Intelligence and Statistics*, pages 837–848. PMLR, 2019.

Adam Paszke, Sam Gross, Francisco Massa, Adam Lerer, James Bradbury, Gregory Chanan, Trevor Killeen, Zeming Lin, Natalia Gimelshein, Luca Antiga, Alban Desmaison, Andreas Kopf, Edward Yang, Zachary DeVito, Martin Raison, Alykhan Tejani, Sasank Chilamkurthy, Benoit Steiner, Lu Fang, Junjie Bai, and Soumith Chintala. Pytorch: An imperative style, high-performance deep learning library. In H. Wallach, H. Larochelle, A. Beygelzimer, F. d'Alché-Buc, E. Fox, and R. Garnett, editors, *Advances in Neural Information Processing Systems 32*, pages 8024–8035. Curran Associates, Inc., 2019.

Dennis Prangle, Michael GB Blum, G Popovic, and SA Sisson. Diagnostic tools for approximate bayesian computation using the coverage property. *Australian & New Zealand Journal of Statistics*, 56(4):309–329, 2014.

Astrid A Prinz, Cyrus P Billimoria, and Eve Marder. Alternative to hand-tuning conductance-based models: construction and analysis of databases of model neurons. *Journal of neurophysiology*, 2003.

Astrid A Prinz, Dirk Bucher, and Eve Marder. Similar network activity from disparate circuit parameters. *Nature neuroscience*, 7(12):1345–1352, 2004.

Stefan T Radev, Ulf K Mertens, Andreas Voss, Lynton Ardizzone, and Ullrich Köthe. Bayesflow: Learning complex stochastic models with invertible neural networks. *IEEE transactions on neural networks and learning systems*, 2020.

Srikanth Ramaswamy, Jean-Denis Courcol, Marwan Abdellah, Stanislaw R Adaszewski, Nicolas Antille, Selim Arsever, Guy Atenekeng, Ahmet Bilgili, Yury Brukau, Athanassia Chalimourda, et al. The neocortical microcircuit collaboration portal: a resource for rat somatosensory cortex. *Frontiers in neural circuits*, 9:44, 2015.

Poornima Ramesh, Jan-Matthis Lueckmann, Jan Boelts, Álvaro Tejero-Cantero, David S. Greenberg, Pedro J. Goncalves, and Jakob H. Macke. GATSBI: Generative adversarial training for simulation-based inference. In *International Conference on Learning Representations*, 2022.

François Rozet et al. Arbitrary marginal neural ratio estimation for likelihood-free inference. *Université de Liège, Liège, Belgique*, 2021.

Donald B Rubin. Using the sir algorithm to simulate posterior distributions. *Bayesian statistics*, 3: 395–402, 1988.

John Skilling. Nested sampling. In *Aip conference proceedings*, volume 735, pages 395–405. American Institute of Physics, 2004.

Sean Talts, Michael Betancourt, Daniel Simpson, Aki Vehtari, and Andrew Gelman. Validating bayesian inference algorithms with simulation-based calibration. *arXiv preprint arXiv:1804.06788*, 2018.

Alvaro Tejero-Cantero, Jan Boelts, Michael Deistler, Jan-Matthis Lueckmann, Conor Durkan, Pedro J. Gonçalves, David S. Greenberg, and Jakob H. Macke. sbi: A toolkit for simulation-based inference. *Journal of Open Source Software*, 5(52):2505, 2020. doi: 10.21105/joss.02505.

Owen Thomas, Ritabrata Dutta, Jukka Corander, Samuel Kaski, and Michael U Gutmann. Likelihood-free inference by ratio estimation. *Bayesian Analysis*, 17(1):1–31, 2022.

Werner Van Geit, Michael Gevaert, Giuseppe Chindemi, Christian Rössert, Jean-Denis Courcol, Eilif B Muller, Felix Schürmann, Idan Segev, and Henry Markram. Bluepyopt: leveraging open source software and cloud infrastructure to optimise model parameters in neuroscience. *Frontiers in neuroinformatics*, page 17, 2016.

Peter J Wangersky. Lotka-volterra population models. *Annual Review of Ecology and Systematics*, 9 (1):189–218, 1978.

Simon N Wood. Statistical inference for noisy nonlinear ecological dynamic systems. *Nature*, 466 (7310):1102–1104, 2010.

Omry Yadan. Hydra - a framework for elegantly configuring complex applications. Github, 2019.

Checklist

1. For all authors...

    (a) Do the main claims made in the abstract and introduction accurately reflect the paper's contributions and scope? [Yes]

    (b) Did you describe the limitations of your work? [Yes]

    (c) Did you discuss any potential negative societal impacts of your work? [N/A]

    (d) Have you read the ethics review guidelines and ensured that your paper conforms to them? [Yes]

2. If you are including theoretical results...

    (a) Did you state the full set of assumptions of all theoretical results? [Yes]

    (b) Did you include complete proofs of all theoretical results? [Yes]

3. If you ran experiments...

    (a) Did you include the code, data, and instructions needed to reproduce the main experimental results (either in the supplemental material or as a URL)? [Yes]

    (b) Did you specify all the training details (e.g., data splits, hyperparameters, how they were chosen)? [Yes]

    (c) Did you report error bars (e.g., with respect to the random seed after running experiments multiple times)? [Yes]

    (d) Did you include the total amount of compute and the type of resources used (e.g., type of GPUs, internal cluster, or cloud provider)? [Yes]

4. If you are using existing assets (e.g., code, data, models) or curating/releasing new assets...

    (a) If your work uses existing assets, did you cite the creators? [Yes]

    (b) Did you mention the license of the assets? [N/A]

    (c) Did you include any new assets either in the supplemental material or as a URL? [N/A]

    (d) Did you discuss whether and how consent was obtained from people whose data you're using/curating? [N/A]

    (e) Did you discuss whether the data you are using/curating contains personally identifiable information or offensive content? [N/A]

5. If you used crowdsourcing or conducted research with human subjects...

    (a) Did you include the full text of instructions given to participants and screenshots, if applicable? [N/A]

    (b) Did you describe any potential participant risks, with links to Institutional Review Board (IRB) approvals, if applicable? [N/A]

    (c) Did you include the estimated hourly wage paid to participants and the total amount spent on participant compensation? [N/A]

6 Appendix

6.1 Reproducibility statement

We used the configuration manager hydra to track the configuration and seeds of each run [Yadan, 2019]. All code to reproduce the results can be found at `https://github.com/mackelab/tsnpe_neurips`. We implemented TSNPE on top of the publicly accessible sbi toolbox [Tejero-Cantero et al., 2020]. All simulations and runs were performed on a high-performance computer. For each run, we used between 8 and 48 CPU cores.

6.2 Proof of convergence

Below, we prove that, for a given observation $\mathbf{x}_o$, the posterior distribution obtained with TSNPE $q_\phi(\boldsymbol{\theta}|\mathbf{x}_o)$ converges to the true posterior distribution $p(\boldsymbol{\theta}|\mathbf{x}_o)$ under the assumption that the HPR_ϵ of the approximate posterior at every TSNPE round covers the support (i.e., the HPR_ϵ for $\epsilon = 0$) of the true posterior given the observation $\mathbf{x}_o$. We call the support of the true posterior $\mathcal{M}$, i.e. $\mathcal{M} = \mathrm{supp}(p(\boldsymbol{\theta}|\mathbf{x}_o))$. The proof proceeds in two steps: First, we derive the effective proposal distribution when pooling data from all rounds. Second, we show that, for such proposal distributions, the neural density estimator converges to the true posterior.

Deriving the proposal distribution   We denote by $\tilde{p}^r(\boldsymbol{\theta})$ the proposal distribution from which $\boldsymbol{\theta}$ are drawn in round r. In the first round, we use the prior, i.e., $\tilde{p}^{r=1}(\boldsymbol{\theta}) = p(\boldsymbol{\theta})$. In later rounds, we sample from the prior but reject samples that lie outside of the HPR_ϵ of the approximate posterior given $\mathbf{x}_o$. The samples drawn in round r are thus drawn from

$$\tilde{p}^r(\boldsymbol{\theta}) = U^r(\boldsymbol{\theta})p(\boldsymbol{\theta})/Z^r, \tag{1}$$

where Z^r is the normalization constant and $U^r(\boldsymbol{\theta})$ is 1 on the HPR_ϵ of the approximate posterior at round r and zero otherwise. Given our assumption that the HPR_ϵ of the approximate posterior covers the support of the true posterior $\mathcal{M}$, $U^r(\boldsymbol{\theta})$ is 1 on the support of the true posterior $\mathcal{M}$.

When pooling simulations from all rounds, after R rounds, the parameters are sampled from a mixture of all proposal distributions:

$$\tilde{p}(\boldsymbol{\theta}) = \frac{1}{N}\sum_{r=1}^{R}\tilde{p}^r(\boldsymbol{\theta}) = p(\boldsymbol{\theta}) \cdot \left(\frac{1}{N}\sum_{r=1}^{R}U^r(\boldsymbol{\theta})/Z^r\right) = p(\boldsymbol{\theta}) \cdot f(\boldsymbol{\theta}). \tag{2}$$

In this equation, we assumed that all rounds contain equally many simulations, but the proof can easily be extended to rounds with different numbers of simulations by adding weights to the above sum.

As can be seen above, the distribution $\tilde{p}(\boldsymbol{\theta})$ is the prior times a function $f(\boldsymbol{\theta})$ which is made up of several steps and whose steps are defined by the HPR_ϵ of the approximate posterior of every round (illustration in Appendix Fig. 23). Finally, under the assumption that all $U^r(\boldsymbol{\theta})$ are 1 on the support of the true posterior $\mathcal{M}$, we have, for any $\boldsymbol{\theta} \in \mathcal{M}$

$$f(\boldsymbol{\theta}) = \frac{1}{N}\sum_{r=1}^{R}U^r(\boldsymbol{\theta})/Z_1^r = \frac{1}{N}\sum_{r=1}^{R}1/Z_1^r = \mathrm{constant} = c,$$

i.e., $f(\boldsymbol{\theta})$ is not a function of $\boldsymbol{\theta}$. Thus, for any $\boldsymbol{\theta} \in \mathcal{M}$, we have

$$\tilde{p}(\boldsymbol{\theta}) = p(\boldsymbol{\theta}) \cdot c \propto p(\boldsymbol{\theta})$$

We emphasise that this proportionality holds only for $\boldsymbol{\theta} \in \mathcal{M}$, but not necessarily for $\boldsymbol{\theta}$ outside of the support of the true posterior.

Training the neural density estimator   Next, we show that, for a proposal distribution of the form derived in the paragraph above, the approximate posterior $q_\phi(\boldsymbol{\theta}|\mathbf{x}_o)$ for an observation $\mathbf{x}_o$ converges to the true posterior distribution $p(\boldsymbol{\theta}|\mathbf{x}_o)$.

TSNPE minimizes the following loss function:

$$\mathcal{L} = -\frac{1}{N} \sum_i \log(q_{\boldsymbol{\phi}}(\boldsymbol{\theta}_i|\mathbf{x}_i))$$

$$\xrightarrow{N \to \infty} -\mathbb{E}_{p(\boldsymbol{\theta},\mathbf{x})}[\log(q_{\boldsymbol{\phi}}(\boldsymbol{\theta}|\mathbf{x}))]$$

$$= -\mathbb{E}_{\tilde{p}(\boldsymbol{\theta})p(\mathbf{x}|\boldsymbol{\theta})}[\log(q_{\boldsymbol{\phi}}(\boldsymbol{\theta}|\mathbf{x}))].$$

Plugging in the proposal distribution defined above:

$$\mathcal{L} = -\iint f(\boldsymbol{\theta})p(\boldsymbol{\theta})p(\mathbf{x}|\boldsymbol{\theta}) \log(q_{\boldsymbol{\phi}}(\boldsymbol{\theta}|\mathbf{x})) \, d\boldsymbol{\theta}d\mathbf{x}$$

$$= \int p(\mathbf{x}) \int -f(\boldsymbol{\theta})p(\boldsymbol{\theta}|\mathbf{x}) \log(q_{\boldsymbol{\phi}}(\boldsymbol{\theta}|\mathbf{x})) \, d\boldsymbol{\theta}d\mathbf{x}.$$

The term within the integral over $\boldsymbol{\theta}$ is proportional to the Kullback-Leibler-divergence between $f(\boldsymbol{\theta})p(\boldsymbol{\theta}|\mathbf{x})/Z$ (with $Z = \int f(\boldsymbol{\theta})p(\boldsymbol{\theta}|\mathbf{x})d\boldsymbol{\theta}$) and the approximate posterior $q_{\boldsymbol{\phi}}(\boldsymbol{\theta}|\mathbf{x})$. Thus, $\mathcal{L}$ is minimized if and only if

$$q_{\boldsymbol{\phi}}(\boldsymbol{\theta}|\mathbf{x}) \propto f(\boldsymbol{\theta})p(\boldsymbol{\theta}|\mathbf{x})$$

for all $\mathbf{x}$ within the the support of $p(\mathbf{x})$ [Papamakarios and Murray, 2016].

This means that, for arbitrary $\mathbf{x} \in \text{supp}(p(\mathbf{x}))$, $q_{\boldsymbol{\phi}}(\boldsymbol{\theta}|\mathbf{x})$ will not converge to the true posterior $p(\boldsymbol{\theta}|\mathbf{x})$, but to $f(\boldsymbol{\theta})p(\boldsymbol{\theta}|\mathbf{x})/Z$. However, for the observed data $\mathbf{x} = \mathbf{x}_o$, we have:

$$q_{\boldsymbol{\phi}}(\boldsymbol{\theta}|\mathbf{x}_o) \propto f(\boldsymbol{\theta})p(\boldsymbol{\theta}|\mathbf{x}_o) = \begin{cases} c \cdot p(\boldsymbol{\theta}|\mathbf{x}_o) & \text{if } \boldsymbol{\theta} \in \mathcal{M} \\ f(\boldsymbol{\theta}) \cdot 0 & \text{else} \end{cases}$$

The first case follows from the fact that $f(\boldsymbol{\theta})$ is constant on the support of the true posterior. The second case follows because the true posterior has zero probability density for $\boldsymbol{\theta}$ outside of its own support $\mathcal{M}$. Thus:

$$q_{\boldsymbol{\phi}}(\boldsymbol{\theta}|\mathbf{x}_o) \propto p(\boldsymbol{\theta}|\mathbf{x}_o).$$

Since $q_{\boldsymbol{\phi}}(\boldsymbol{\theta}|\mathbf{x}_o)$ is a (conditional) normalizing flow, it is normalized and, thus:

$$q_{\boldsymbol{\phi}}(\boldsymbol{\theta}|\mathbf{x}_o) = p(\boldsymbol{\theta}|\mathbf{x}_o).$$

6.3 Simulation-based coverage calibration (SBCC)

The algorithm for computing the coverage (SBCC) is shown in Alg. 2.

Algorithm 2: Simulation-based coverage calibration (SBCC)

Inputs: proposal $\tilde{p}(\boldsymbol{\theta})$, approximate posterior $q_{\boldsymbol{\phi}}$ trained on $\boldsymbol{\theta} \sim \tilde{p}(\boldsymbol{\theta})$, number of simulations M, number of posterior samples per simulation P. Database of empirical coverages $\mathcal{E}$, initialized as the empty set.
Outputs: Coverage for different confidence levels $1 - \alpha$.
for $i \in [1, ..., M]$ **do**
    $\boldsymbol{\theta}_i^* \sim \tilde{p}(\boldsymbol{\theta})$
    simulate $\mathbf{x}_i^* \sim p(\mathbf{x}|\boldsymbol{\theta}_i^*)$
    $l_i^* = \log(q_{\boldsymbol{\phi}}(\boldsymbol{\theta}_i^*|\mathbf{x}_i^*))$;   `// compute log-prob of ground-truth`
    $c = 0$
    for $j \in [1, ..., P]$ **do**
        $\boldsymbol{\theta}_j \sim q_{\boldsymbol{\phi}}(\boldsymbol{\theta}|\mathbf{x}_i^*)$
        $l_j = \log(q_{\boldsymbol{\phi}}(\boldsymbol{\theta}_j|\mathbf{x}_i^*))$;   `// compute log-probs of posterior samples`
        if $l_j > l_i^*$ **then**
            $c = c + 1$
        $e = c/P$;   `// fraction of posterior samples whose log-prob is larger`
          `than ground-truth log-prob`
        add e to $\mathcal{E}$
Plot CDF of $\mathcal{E}$

Algorithm 3: Obtaining the HPR$_\epsilon$ of the approximate posterior and sampling the truncated proposal with rejection sampling

---

Inputs: Prior $p(\boldsymbol{\theta})$, Approximate posterior q_ϕ, observation $\mathbf{x}_o$, number of posterior samples M, ϵ that defines the HPR, number of desired samples from $\tilde{p}(\theta)$ N. Database of log-probabilities $\mathcal{P}$, initialized as an empty set.
Outputs: Samples $\mathcal{S}$ from truncated proposal $\tilde{p}(\boldsymbol{\theta})$.
for $i \in [1, ..., M]$ **do**
   | $\boldsymbol{\theta}_i \sim q_\phi(\boldsymbol{\theta}|\mathbf{x}_o)$
   | $l_i = \log(q_\phi(\boldsymbol{\theta}_i|\mathbf{x}_o)$
   | add l_i to $\mathcal{P}$
$\boldsymbol{\kappa} = \text{quantile}_\epsilon(\mathcal{P})$;   `// threshold for HPR`$_\epsilon$

`// sample truncated proposal with rejection sampling`
while $s < N$ **do**
   | $\boldsymbol{\theta} \sim p(\boldsymbol{\theta})$
   | $l = \log(q_\phi(\boldsymbol{\theta}|\mathbf{x}_o))$
   | **if** $l > \boldsymbol{\kappa}$ **then**
   | | add $\boldsymbol{\theta}$ to $\mathcal{S}$
   | | s += 1

6.4 Algorithm description for sampling from the HPR of the approximate posterior

The algorithm for sampling from the HPR$_\epsilon$ of the approximate posterior is shown in Alg. 3.

6.5 Alleviating issues of APT

We compared TSNPE to Automatic Posterior Transformation (APT) [Greenberg et al., 2019]. In this section, we briefly review how APT works, and why 'leakage' occurs, and how we attempted to improve it.

APT review Broadly, APT exists in two versions. Its first version can be applied only if the density estimator $q_\phi(\boldsymbol{\theta}|\mathbf{x})$ is a mixture of Gaussians, the proposal $\tilde{p}(\boldsymbol{\theta})$ is a mixture of Gaussians, and the prior $p(\boldsymbol{\theta})$ is either uniform or Gaussian. We did not compare TSNPE to APT in this form because we wanted to use more expressive density estimators for $q_\phi(\boldsymbol{\theta}|\mathbf{x})$. The second version of APT, known as atomic APT, allows to use any density estimator $q_\phi(\boldsymbol{\theta}|\mathbf{x})$, any proposal $\tilde{p}(\boldsymbol{\theta})$ and any explicit prior $p(\boldsymbol{\theta})$. One must be able to evaluate the density estimator and the prior, but the proposal can be implicit (i.e., without closed form density). Atomic APT minimizes the loss:

$$\mathcal{L}_\phi = -\frac{1}{N} \sum_{i=1}^{N} \log \frac{q_\phi(\boldsymbol{\theta}_i|\mathbf{x}_i)/p(\boldsymbol{\theta}_i)}{q_\phi(\boldsymbol{\theta}_i|\mathbf{x}_i)/p(\boldsymbol{\theta}_i) + \sum_{j=1...A-1} q_\phi(\boldsymbol{\theta}_j|\mathbf{x}_i)/p(\boldsymbol{\theta}_j)}$$

with number of atoms A. In this loss, $\boldsymbol{\theta}_j$ and $\boldsymbol{\theta}_i$ can be sampled from *any* proposal distribution. $\mathbf{x}_i$ is sampled from $p(\mathbf{x}|\boldsymbol{\theta}_i)$.

Leakage issue Notice that the above loss is the same for $q_\phi(\boldsymbol{\theta}|\mathbf{x})$ and for $c \cdot q_\phi(\boldsymbol{\theta}|\mathbf{x})$. In other words, the approximate posterior has to be correct only up to a proportionality constant [Greenberg et al., 2019, Durkan et al., 2020]. Thus, an approximate posterior $q_\phi(\boldsymbol{\theta}|\mathbf{x})$ which is $c \cdot p(\boldsymbol{\theta}|\mathbf{x})$ will have a minimal loss. Since the dataset on which $q_\phi(\boldsymbol{\theta}|\mathbf{x})$ is trained contains no $\boldsymbol{\theta}$ that lies outside of the prior bounds, the approximate posterior can be anything outside of the prior bounds without affecting the value of the loss function. This is what is called 'leakage', and which has been pointed out as a potential problem both in the original APT paper Greenberg et al. [2019] and work studying the relationship of APT with contrastive learning approaches Durkan et al. [2020]: While the approximate posterior might be proportional to the true posterior within the bounds of the prior $p(\boldsymbol{\theta})$, it can put significant mass outside of the prior bounds (because the loss does not penalize this behaviour).

Transforming the parameter space We tried to fix the leakage issue by appending a transformation such that the density estimator has constrained support. This requires that the bounds of

the parameter space are known and that such a transformation can be implemented. If this fix can be applied, the leakage will be zero by definition. In all our experiments, such a transformation substantially helped with the leakage problem.

Leakage into regions of no training data   However, even when possible, such transformation does not completely prevent 'leakage': When inspecting the loss of APT, we see that the approximate posterior can put mass into any region of the parameter space in which no parameter sets $\boldsymbol{\theta}$ in the training data lie. For example, if the prior distribution is standard Gaussian and one trains APT on 100 parameter sets sampled from the prior, the training dataset will unlikely contain values that are smaller than -3 or larger than 3. Therefore, APT can 'leak' into the regions below -3 or above 3 and still have an optimal loss. While, in the limit of infinite data, APT would correct its 'leakage' as soon as parameters from these regions are used as training data, given a finite number of simulations, the approximate posterior can 'leak' into new regions which have not been explored (yet). The (potential) problem of leakage does not affect all applications equally: High-dimensional parameter spaces suffer more from this behavior than low-dimensional ones, as there are many regions into which the mass of the approximate posterior can 'leak'. This behaviour is illustrated in Appendix Fig. 17.

Leakage because of invalid data   Another way in which leakage can occur is if the simulator produces invalid data (e.g. NaN or infinity). Often, such invalid simulations are discarded from the training dataset [Lueckmann et al., 2017] and the approximate posterior is trained only on samples that produce valid outputs. For example, assume that a small region of the prior always produces invalid simulations. In this case, the approximate posterior will never be trained on simulations from this parameter region and APT can 'leak' into this region. Thus, the approximate posterior might contain significant mass in parameter regions that produce invalid simulations.

Explicit recommendations for running APT   We will now give explicit recommendations for running APT. These modification greatly improved the performance of APT in our experiments, but were not able to avoid the failure of the algorithm on challenging real-world problems such as the pyloric network (Fig. 5).

1. For priors with bounded supports: If possible, transform the parameter space into unbounded space.

2. Do not discard invalid simulations. Instead, replace invalid entries (such as NaN) with a substantially different value than the observed data and train on all available simulations.

3. Check if the posterior contains a lot of mass in regions with very low prior probability. If this is the case, it can hint at a failure of APT through leakage into regions of no training data.

4. If you transformed the parameter space, check if many posterior samples lie very close to the bounds. Again, this can hint at a failure of APT through leakage into regions of no training data.

6.6   Relation between simulation-based calibration and our diagnostic

As discussed above, our method is closely related to simulation-based calibration (SBC) [Cook et al., 2006, Talts et al., 2018]. Briefly, SBC samples $\boldsymbol{\theta}^*$ from the prior, samples the likelihood $\mathbf{x}^* \sim p(\mathbf{x}|\boldsymbol{\theta}^*)$ and then draws samples from the posterior $\boldsymbol{\theta}_i \sim p(\boldsymbol{\theta}|\mathbf{x}^*)$ (e.g., with MCMC). It then projects the (potentially high-dimensional) parameters $\boldsymbol{\theta}_i$ into a one-dimensional space $T(\boldsymbol{\theta}_i)$. Often, this projection is the 1D-marginal distribution of parameters [Carpenter et al., 2017]. It then ranks $T(\boldsymbol{\theta}^*)$ under all posterior samples $T(\boldsymbol{\theta}_{1\ldots N})$. Repeated across several prior samples, the distribution of ranks should be uniform. For high-dimensional parameter spaces, the marginal distribution of each parameter is checked independently.

Notably, other projections into a one-dimensional space are possible. Below, we explain that our method is identical to running SBC with projection $T : \boldsymbol{\theta} \rightarrow q_\phi(\boldsymbol{\theta}|\mathbf{x})$ and with posterior samples exactly following $q_\phi(\boldsymbol{\theta}|\mathbf{x})$.

In SBC and in our diagnostic method, samples are drawn from the prior $\boldsymbol{\theta}^* \sim p(\boldsymbol{\theta})$ and simulated $\mathbf{x}^* \sim p(\mathbf{x}|\boldsymbol{\theta})$. In our diagnostic method, as well as in SBC with projection being the log-probability

of the approximate posterior, one then samples the posterior to obtain $\boldsymbol{\theta}_i$ and evaluates the log-probability of all samples, i.e., $l_i = T(\boldsymbol{\theta}_i) = \log(q(\boldsymbol{\theta}_i|\mathbf{x}^*)$ as well as of the initial parameter set $l^* = \log(q(\boldsymbol{\theta}^*|\mathbf{x}^*)$. SBC then ranks l^* under all l_i, which is equivalent to computing its quantile (as in our method). In our diagnostic tool, one then evaluates whether this quantile is above or below several confidence levels (evaluation on a 1D evenly spaced grid, same as rank binning in SBC). This generates a step-function with the step occuring at the quantile of l^*. This step function is the cumulative distribution function of a dirac at the quantile of l^*. Therefore, repeated across several $\boldsymbol{\theta}^*$, our coverage plots (e.g., Fig 3c) correspond to the cumulative distribution function of the histograms generated by SBC (with projection $T : \boldsymbol{\theta} \rightarrow \log(q_\phi(\boldsymbol{\theta}|\mathbf{x}))$ and posterior samples exactly following $q_\phi(\boldsymbol{\theta}|\mathbf{x})$).

6.7 SBCC in a multi-round setting

We run our diagnostic tool after every round of training. If one trains only on simulations that were run in the most recent round, SBCC can be run as in the first round. However, if one wishes to train on simulations from all rounds, then the deep neural density estimator converges to:

$$q_\phi(\boldsymbol{\theta}|\mathbf{x}) \propto f(\boldsymbol{\theta})p(\boldsymbol{\theta}|\mathbf{x}).$$

Proof in Sec. 6.2. As is described in Sec. 6.2, this means that $q_\phi(\boldsymbol{\theta}|\mathbf{x})$ will not converge to the true posterior for arbitrary $\mathbf{x}$, but only for the observation $\mathbf{x}_o$.

This poses a problem for SBCC: As described in Alg. 2, SBCC measures whether the coverage is correct (on average) for many $\mathbf{x}$ generated by the proposal distribution. Since the loss employed by TSNPE only ensures convergence for $\mathbf{x}_o$, it will by construction not provide correct results for other $\mathbf{x}$.

This issue can be solved in two ways:

1. When running SBCC, instead of drawing samples from the proposal prior of the most recent round $\tilde{p}^r(\boldsymbol{\theta})$, one can draw samples $\boldsymbol{\theta}^*$ from $\tilde{p}(\boldsymbol{\theta})$, i.e., the distribution that emerges from pooling data from all rounds (notation as in Sec. 6.2 and Alg. 2). This is the method described in Appendix Alg. 2.

2. One can truncate the approximate posteriors $q_\phi(\boldsymbol{\theta}|\mathbf{x}^*)$ while running SBCC (see Alg. 2 for notation). With this strategy, when running SBCC in round r, we draw parameters from $\boldsymbol{\theta}^* \sim \tilde{p}^r(\boldsymbol{\theta})$ (the truncated proposal from round r), simulate them $\mathbf{x}^* \sim p(\mathbf{x}|\boldsymbol{\theta}^*)$, sample from the posterior $\boldsymbol{\theta}_i \sim q_\phi(\boldsymbol{\theta}|\mathbf{x}^*)$, reject samples that lie outside of $\text{HPR}_\epsilon(q_\phi(\boldsymbol{\theta}_i|\mathbf{x}_o))$, and then continue as described in Alg. 2. Strategy 2 only ensures that the posterior regions which lie within $\text{HPR}_\epsilon(q_\phi(\boldsymbol{\theta}|\mathbf{x}_o))$ are well-calibrated. It does not ensure that the full posterior ($q_\phi(\boldsymbol{\theta}|\mathbf{x}^*)$ with $\mathbf{x}^* \sim p(\mathbf{x}^*|\boldsymbol{\theta}^*)$ and $\boldsymbol{\theta}^* \sim \tilde{p}^r(\boldsymbol{\theta})$) is well-calibrated.

6.8 Toy model

The toy model shown in Fig. 1 is given by a uniform prior within $[-2, -1]$ and $[1, 2]$. The simulator is $x \sim \theta^2 + \epsilon$, where ϵ is a Gaussian distribution with mean zero and standard deviation 0.2. We ran APT [Greenberg et al., 2019] and TSNPE for 5 rounds with 500 simulations per round. For APT, all hyperparameters are the default values from the sbi package [Tejero-Cantero et al., 2020], but we used a neural spline flow (NSF) for both APT and TSNPE [Durkan et al., 2019].

6.9 Benchmark tasks

Below, we briefly describe the benchmark tasks. For details, please see Lueckmann et al. [2021].

Gaussian linear: 10 parameters which are the mean of a Gaussian model. The prior is Gaussian, resulting in a Gaussian posterior.

Bernoulli GLM: Generalized linear model with Bernoulli observations. Inference is performed on 10-dimensional sufficient summary statistics of the originally 100 dimensional raw data. The resulting posterior is 10-dimensional, unimodal, and concave.

Lotka Volterra: A traditional model in ecology [Wangersky, 1978], which describes a predator-prey interaction between species, illustrating a task with complex likelihood and unimodal posterior.

SLCP: A task introduced by Papamakarios et al. [2019] with a simple likelihood and complex posterior. The prior is uniform, the likelihood has Gaussian noise but is non-linearly related to the parameters, resulting in a posterior with four symmetrical modes.

Two moons: This model has two parameters with a uniform prior. The simulator is non-linear, generating a posterior with both local and global (bimodal) structure [Greenberg et al., 2019].

SIR: Epidemiological model with two parameters and ten summary statistics [Kermack and McKendrick, 1927].

6.10 Errors due to truncation

As described in Appendix Sec. 6.2, the approximate posterior converges to the true posterior if the truncated proposal covers the support of the true posterior. The truncated support is defined as the high probability region that contains 1-ϵ of mass of the approximate posterior (HPR$_\epsilon$). For $\epsilon > 0$, the HPR$_\epsilon$ will likely not be a superset of the support of the true posterior and hence, there will be errors in posterior approximation. In this section, we discuss the effect of these errors on inference accuracy.

When the value of ϵ is chosen too large, the tails of the approximate posterior are excluded from the truncated proposal. In the following training round, the approximate posterior converges to a distribution that is correct, up to proportionality, within the HPR$_\epsilon$ of the previous approximate posterior, but that underestimates the tails of the posterior distribution. We demonstrate this behavior in Appendix Fig. 11 for a linear Gaussian simulator, uniform prior, 50k simulations per round, and a neural spline flow with 20 bins as neural density estimator. After round 1, the approximate posterior closely matches the true posterior (Fig. 11a). When using a large ϵ, e.g., $\epsilon = 0.1$, the proposal for the second round is narrower than the true posterior and, thus, the proposal obtained by pooling data from both rounds is not constant on the support of the true posterior (Fig. 11b, blue). This leads to the approximate posterior underestimating the tails of the true posterior (Fig. 11b, purple). When using a smaller ϵ, e.g., $\epsilon = 0.01$, the errors induced by truncation become small and inference errors are mostly due to finite data and imperfect convergence of the neural network (Fig. 11c). We note that, throughout our study, we evaluated $\epsilon = \{10^{-3}, 10^{-4}, 10^{-5}\}$, i.e., values that are at least one order of magnitude smaller than $\epsilon = 0.01$.

Overall, this analysis demonstrates that the truncation performed by TSNPE can negatively impact inference quality in the tails of the posterior distribution. We, thus, do not recommend TSNPE in scenarios in which users are particularly interested in the tails of the posterior. In all our benchmark tasks, however, we did not find that the truncation negatively impacted inference quality as measured by C2ST accuracy (Fig. 4, Appendix Fig. 8, Fig. 8). This indicates that, for many (real-world) tasks, the errors due to truncation are outweighed by errors due to finite simulation budgets or imperfect convergence of neural network training.

6.11 Computational cost of rejection sampling and SIR

In this section, we quantify the computational costs of rejection sampling and sampling-importance resampling (SIR). The computational cost of both sampling methods comprises the computational cost of sampling and evaluating the approximate posterior. On an AMD Ryzen Threadripper 1920X 12-Core Processor, drawing (or evaluating) 100k samples takes approximately 10 seconds. On a GeForce RTX 2080 GPU, drawing (or evaluating) 100k samples takes approximately 0.17 seconds. Thus, in SIR (with an oversampling factor $K = 1024$), one can draw (or evaluate) 100 samples from the truncated proposal in 0.17 seconds on a GPU (versus 10 seconds on a CPU). For most real-world simulators, this constitutes a small fraction of the compute time required to simulate the model: e.g., for the multicompartment model, a single simulation takes approximately 30 seconds and, thus, SIR sampling from the truncated support takes up only 0.012% of the total compute time with a GPU. For rejection sampling, the time required to draw samples from the truncated support depends on the rejection rate. However, as long as the acceptance rate is above 0.001%, the cost of rejection sampling is still small compared to the cost of running the simulator.

6.12 Accuracy of SIR

Here, we investigate the (potential) error induced by using sampling-importance resampling (SIR). SIR is an approximate sampling technique and does not produce exact samples for finite K. This

raises the question of how strongly the errors induced by SIR influence the results of TSNPE. In order to investigate this, we performed three analyses: 1) We ran all benchmarking tasks with SIR and $K = 1024$ and compared the results to rejection sampling. Across all benchmark tasks, the performance of TSNPE with SIR matches the performance of TSNPE with rejection sampling (Appendix Fig. 10). 2) In a simple 1D toy model, we investigated how closely the samples produced by SIR match the samples produced by rejection sampling. As can be seen in Appendix Fig. 12, the distribution of SIR samples is quite different from rejection sampling for $K = 16$ and $K = 64$. However, for $K = 1024$, the distribution of samples from SIR very closely matches the distribution of rejection samples. 3) Finally, we investigated the performance of SIR by inspecting the effective sample size (ESS), which we computed as

$$\text{ESS} = 1 / \sum_i^K w_i^2$$

with w_i being the normalized importance weights [Kong, 1992, Djuric et al., 2003, Martino et al., 2017]. For $K = 1024$, across all benchmark tasks, the ESS was on average 25.154 and was never below 2.547, i.e. it was always significantly higher than 1 (the number of resampled samples). All of these results indicate that SIR is expected to be a useful and robust sampling method for TSNPE.

6.13 Pyloric network model

For the pyloric network model, we used the same prior, simulator, and summary statistics as previous work [Gonçalves et al., 2020, Deistler et al., 2021, Glöckler et al., 2022]. The model has a total of 31 parameters and 18 summary statistics. We replaced invalid summary statistics with a value that is 2 standard deviations (of prior predictives) below the observation. The experimental data [Haddad and Marder, 2021] is also the same as used in these previous works.

6.14 Multicompartment model of a single neuron

We performed Bayesian inference in a complex model of single-neuron dynamics. The model is the same as used in Van Geit et al. [2016]. We added observation noise with standard deviations taken from previously published measurements [Hay et al., 2011]. The prior is a uniform distribution within the same bounds as previously used [Van Geit et al., 2016]. The parameters are shown in Table 1. The summary statistics are also the same as in Van Geit et al. [2016].

We replaced NaN values by the minimal value among prior samples minus two standard deviations of prior samples. Several summary statistics had heavy tailed distributions, which led to very high standard deviations. For these summary statistics, we picked the replacement value by hand. The final values are shown in Table 2.

6.15 Choices of hyperparameters

For the results on the benchmark tasks, we picked the same hyperparameters for TSNPE as those that were used in Lueckmann et al. [2021] for APT (called SNPE in Lueckmann et al. [2021]).

For both neuroscience tasks, we used a neural spline slow (NSF) as density estimator [Durkan et al., 2019]. The hyperparameters of the NSF are the defaults from the 'sbi' package [Tejero-Cantero et al., 2020]. On both of these tasks, we used $\epsilon = 10^{-3}$. All other hyperparameters are the defaults from the 'sbi' package with one exception: We used a batchsize of 500 (instead of the default value 50).

For the pyloric network task, we ran APT with 2 atoms. We reduced the number of atoms from the default value in the 'sbi' package (10 atoms) because a larger number of atoms increased training time. When using 10 atoms, the training time exceeded the simulation time of the model on the pyloric network task. With 2 atoms, the training time of APT was comparable to the training time of TSNPE (albeit still a bit higher). We implemented the transformation of the parameter space with the pytorch method 'biject_to()' [Paszke et al., 2019]. For TSNPE, we initially sampled from the truncated proposal with rejection sampling. After the eighth round of training, the rejection rate became exceedingly high and we switched sampling importance resampling (SIR, with $K = 1024$ see Sec. 3.2).

For the multicompartment model of single-neuron dynamics, we initially sampled parameters from the truncated proposal with rejection sampling and switched to SIR after the third round. For this

Index	Parameter	Ground truth
θ_1	gnats2_tbar_nats2_t_apical	0.026145
θ_2	gskv3_1bar_skv3_1_apical	0.004226
θ_3	gimbar_im_apical	0.000143
θ_4	gnata_tbar_nata_t_axonal	3.137968
θ_5	gk_tstbar_k_tst_axonal	0.089259
θ_6	gamma_cadynamics_e2_axonal	0.00291
θ_7	gnap_et2bar_nap_et2_axonal	0.006827
θ_8	gsk_e2bar_sk_e2_axonal	0.007104
θ_9	gca_hvabar_ca_hva_axonal	0.00099
θ_{10}	gk_pstbar_k_pst_axonal	0.973538
θ_{11}	gskv3_1bar_skv3_1_axonal	1.021945
θ_{12}	decay_cadynamics_e2_axonal	287.19873
θ_{13}	gca_lvastbar_ca_lvast_axonal	0.008752
θ_{14}	gamma_cadynamics_e2_somatic	0.000609
θ_{15}	gskv3_1bar_skv3_1_somatic	0.303472
θ_{16}	gsk_e2bar_sk_e2_somatic	0.008407
θ_{17}	gca_hvabar_ca_hva_somatic	0.000994
θ_{18}	gnats2_tbar_nats2_t_somatic	0.983955
θ_{19}	decay_cadynamics_e2_somatic	210.48529
θ_{20}	gca_lvastbar_ca_lvast_somatic	0.000333

Table 1: L5PC parameters.

task, in the first round of training, we used an ensemble of 10 neural networks. From the second round onward we used only a single neural network. For all other runs (toy example, benchmark, pyloric network), we did not use ensembles but always trained only a single network.
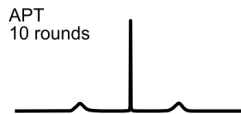
Figure 7: **APT performance after 10 rounds.** Same setup as in Fig. 1, but after running APT for 10 rounds. Leakage gets worse when additional rounds are run.

Summary statistic	Observation	Replacement value
step1_soma_ahp_depth_abs	-62.1358	-110.974
step1_soma_ahp_depth_abs_slow	-62.2882	-151.52
step1_soma_ahp_slow_time	0.140599	-0.8473
step1_soma_ap_height	28.43591	-33.959
step1_soma_ap_width	0.67857	-2.132
step1_soma_isi_cv	0.03328	-1.202
step1_soma_adaptation_index2	-0.0039499	-0.3790
step1_soma_doublet_isi	67.00	-1.699
step1_soma_mean_frequency	7.106	-52.343
step1_soma_time_to_first_spike	33.3000	-719.1
step2_soma_ahp_depth_abs	-60.6933	-110.974
step2_soma_ahp_depth_abs_slow	-60.8186	-151.066
step2_soma_ahp_slow_time	0.1496	-0.8481
step2_soma_ap_height	26.5820	-33.958
step2_soma_ap_width	0.67058	-2.1747
step2_soma_isi_cv	0.03598	-1.0649
step2_soma_adaptation_index2	-0.001467	-0.47684
step2_soma_doublet_isi	44.600	-1.6999
step2_soma_mean_frequency	8.8444	-67.842
step2_soma_time_to_first_spike	23.000	-719.1
step3_soma_ahp_depth_abs	-56.759	-110.744
step3_soma_ahp_depth_abs_slow	-55.903	-149.126
step3_soma_ahp_slow_time	0.2168	-0.83586
step3_soma_ap_height	16.968	-34.01
step3_soma_ap_width	0.5968	-2.6932
step3_soma_isi_cv	0.09933	-1.1164
step3_soma_adaptation_index2	0.007206	-0.5326
step3_soma_doublet_isi	21.100	-1.699
step3_soma_mean_frequency	16.086	-125.30
step3_soma_time_to_first_spike	10.600	-719.1
bap_dend1_ap_amplitude_from_voltagebase	53.267	-60.701
bap_dend2_ap_amplitude_from_voltagebase	30.592	-31.779
bap_soma_ap_height	37.519	-33.95
bap_soma_ap_width	0.800	-1.583
bap_soma_spikecount	1.0	-0.8855

Table 2: L5PC summary statistics.
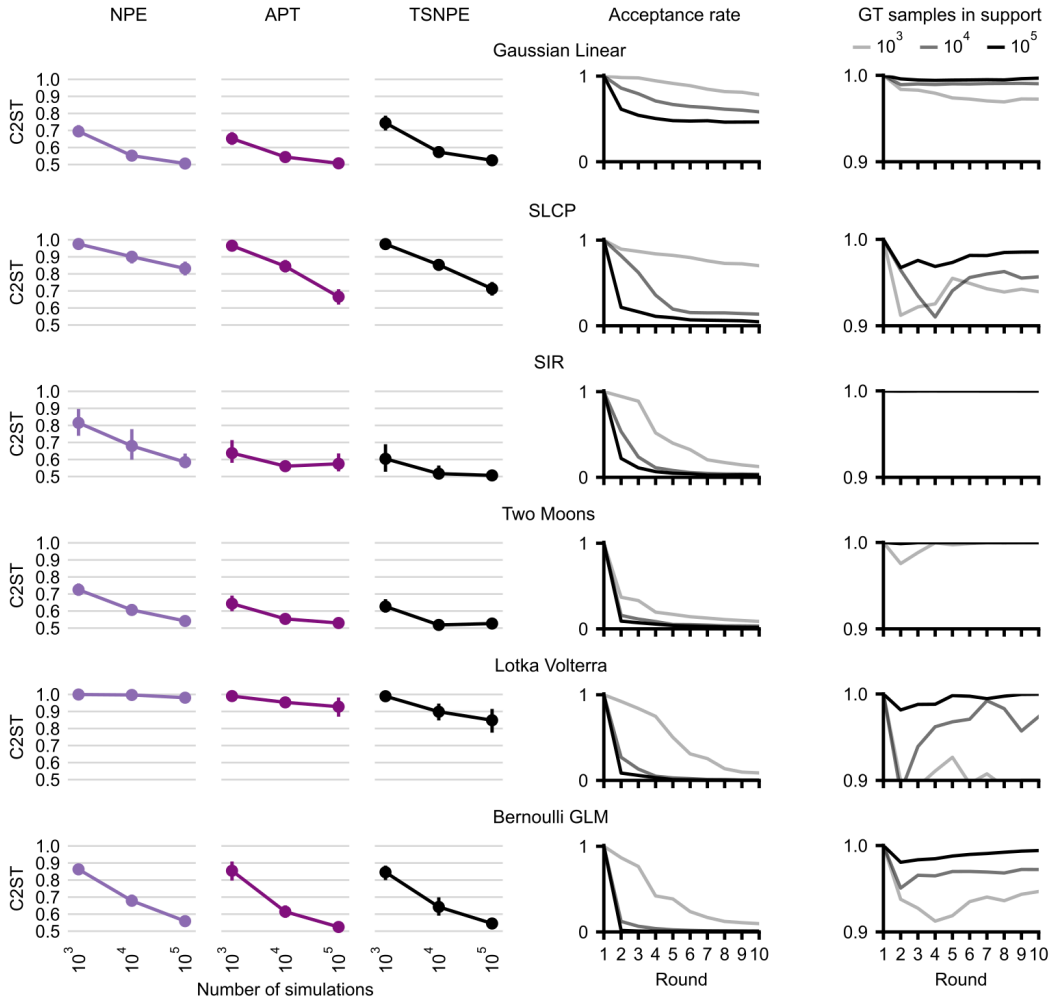
Figure 8: **Benchmark results for a less conservative threshold.** All hyperparameters are the same as in Fig. 4. The only difference is that we used $\epsilon = 10^{-3}$ (compared to 10^{-4} in Fig. 4).
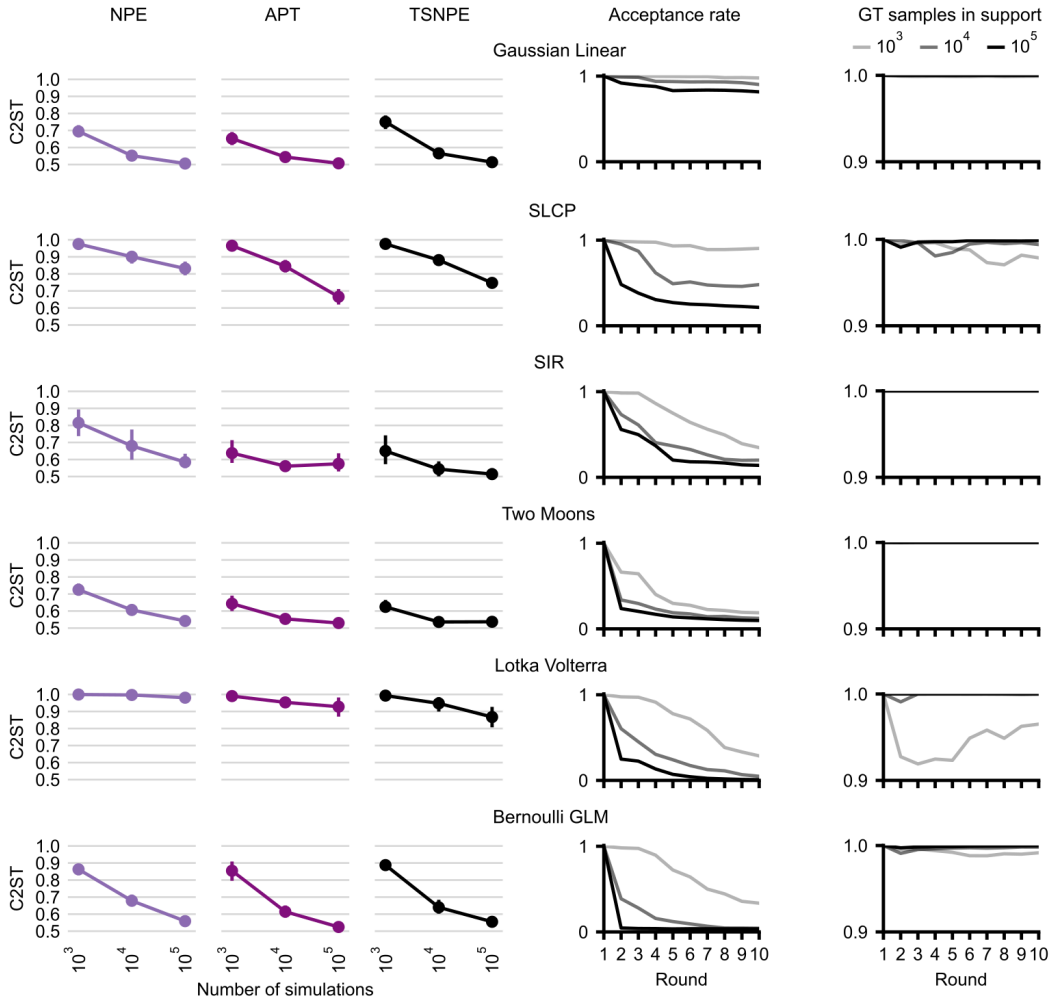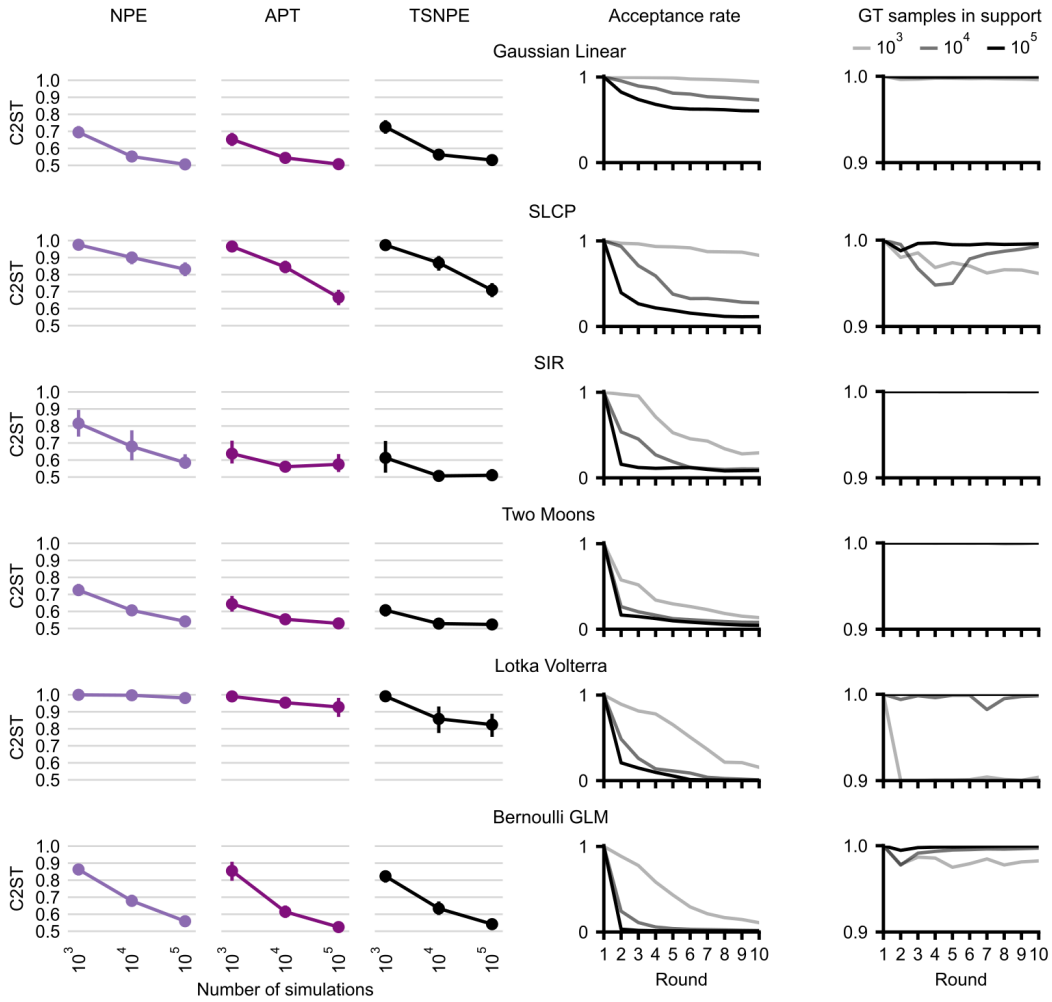
Figure 9: **Benchmark results for a more conservative threshold.** All hyperparameters are the same as in Fig. 4. The only difference is that we used $\epsilon = 10^{-5}$ (compared to 10^{-4} in Fig. 4).

Figure 10: **Benchmark results for sampling importance resampling (SIR).** All hyperparameters are the same as in Fig. 4 ($\epsilon = 10^{-4}$) but we use SIR to sample from the truncated proposal (instead of rejection sampling in Fig. 4).
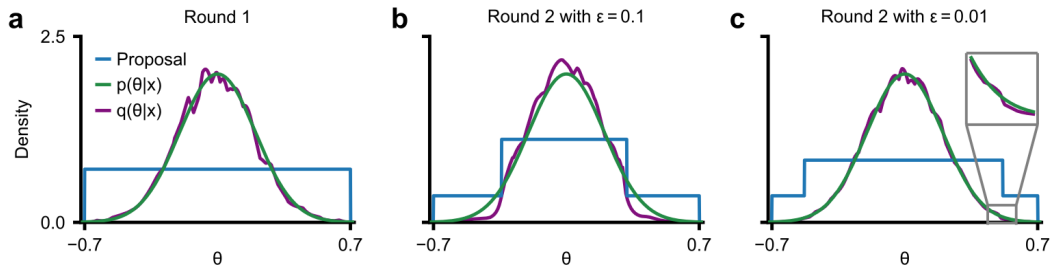
Figure 11: **Errors induced by truncation.** Inference in a linear Gaussian toy model with uniform prior. (a) The approximate posterior after round 1 closely matches the true posterior. (b) For a large truncation value $\epsilon = 0.1$, the approximate posterior after round 2 systematically underestimates the tails of the true posterior distribution. (c) For a smaller truncation value $\epsilon = 0.01$, the error induced by truncation is small.
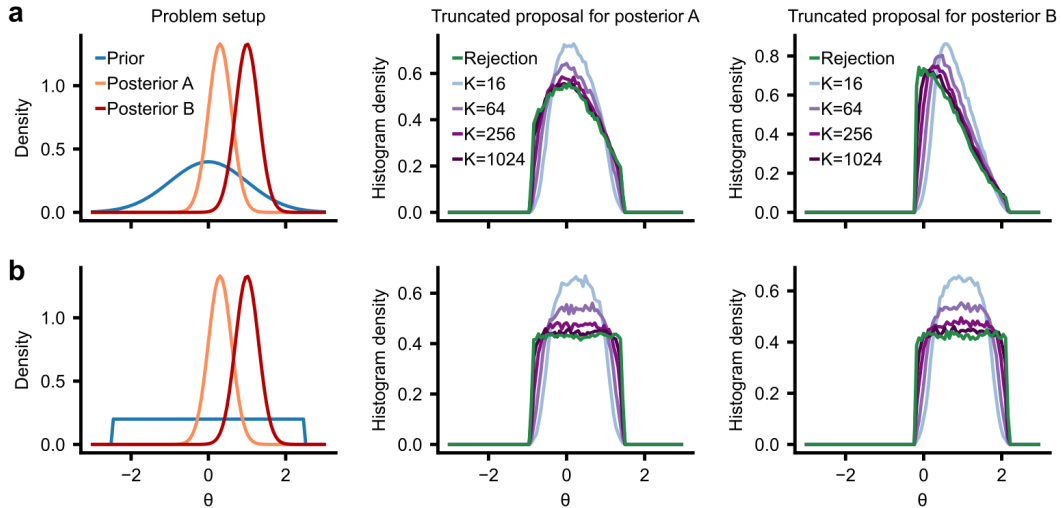
Figure 12: **Comparison of truncated proposal between rejection and importance sampling.** (a) Left: Gaussian prior as well as two posteriors. Middle: Density of 100k samples from the truncated proposal for posterior A. Green is rejection sampling, purple shaded colors are SIR with different oversampling factors K. Right: Same as middle, but for posterior B. (b) Same as panel a, but for a uniform prior.
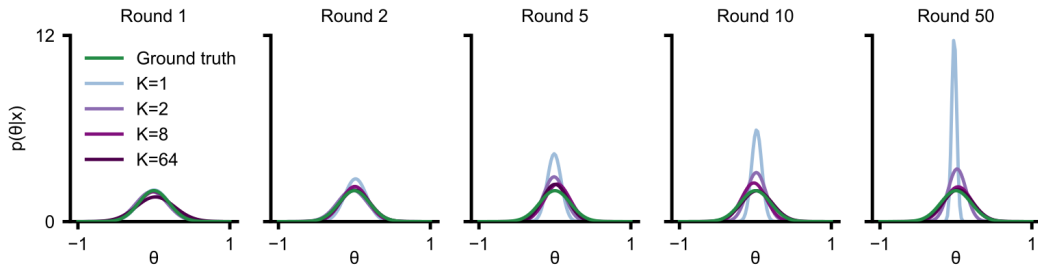
Figure 13: **Poor hyperparameter choices can lead SIR to diverge.** We applied TSNPE to a model with uniform prior (in [-1, 1]) and a linear Gaussian simulator. In each round, we ran 500 simulations, trained only on data from the most recent round, and used a Gaussian approximate posterior. We sampled from the truncated proposal with SIR (with different oversampling factors K). As more rounds are being run, the TSNPE approximate posterior can become too narrow for small K. Larger values of K are robust across 50 rounds.
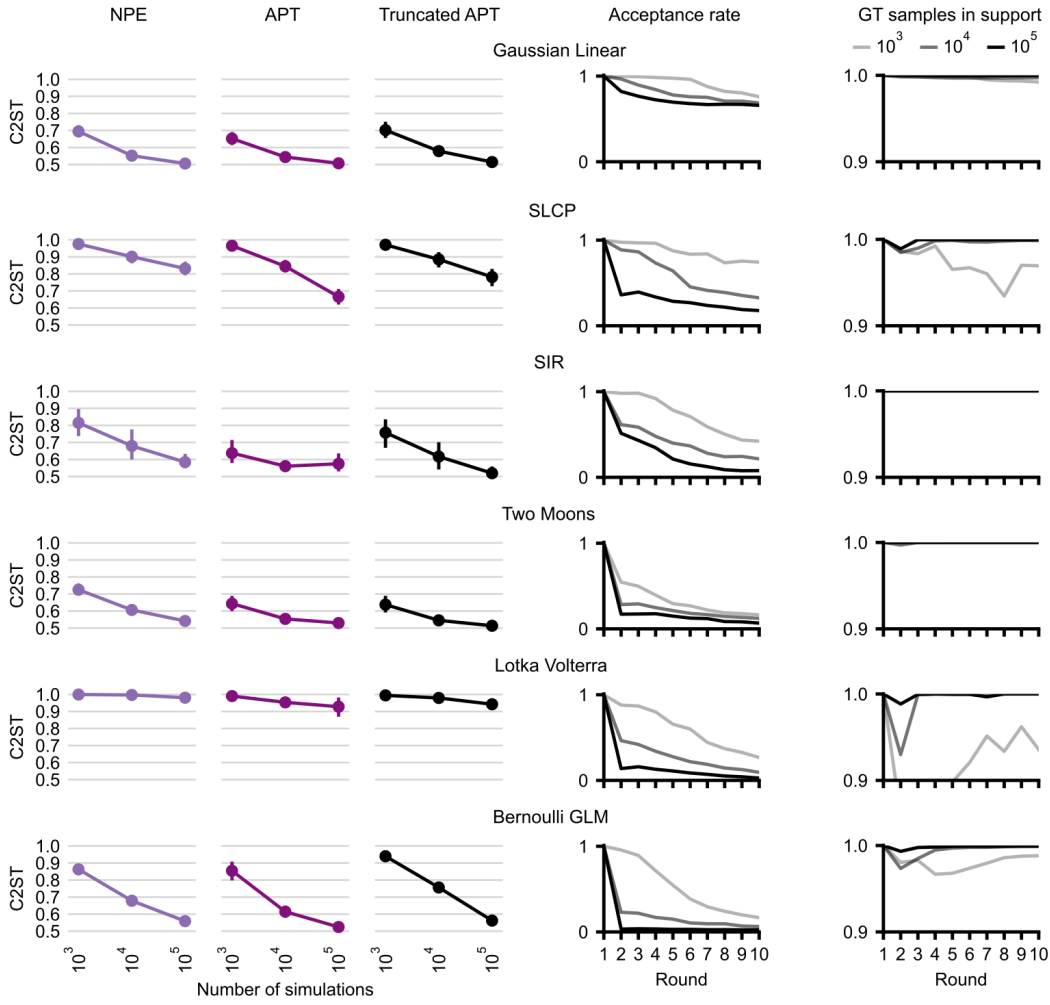
Figure 14: **Comparison between APT and truncated APT.** In order to investigate the effect of the truncated proposals on inference quality, we evaluated two versions of APT: In one scenario (middle column), we draw proposal samples from the previously estimated posterior, whereas in the second scenario (right column), we draw proposal samples from the truncated prior (with $\epsilon = 10^{-4}$). In both versions, we used the atomic loss function proposed in Greenberg et al. [2019]. Therefore, all differences stem from the different proposals. We also compare to standard NPE (trained with maximum-likelihood loss, left column). The two columns on the right are the same as in Fig. 4, evaluated for truncated APT.
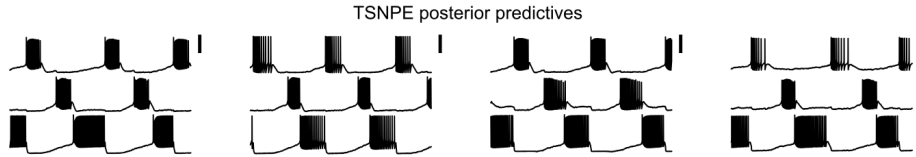
Figure 15: **Four posterior predictives of TSNPE applied to the pyloric network model.** The generated activity closely matches the summary statistics of the experimental data (Fig. 5a).
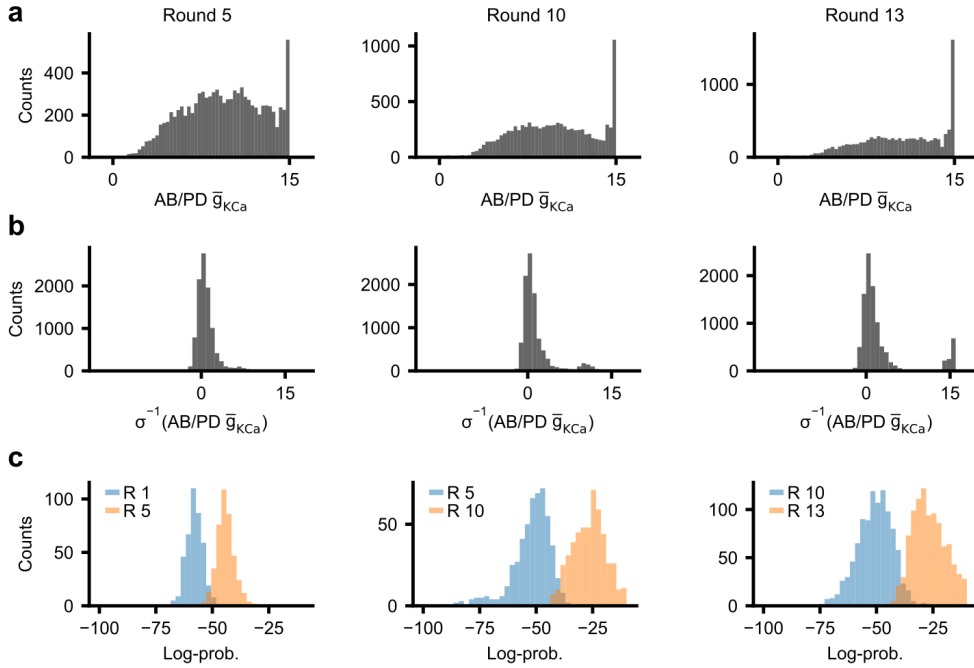
Figure 16: **Further explanation of issues when the parameter space is constrained.** (a) Marginal distribution of $\overline{g}_{KCa}$ of the AB/PD neuron when running APT for 5, 10, and 13 rounds. (b) Marginal distribution of this parameter, but when transformed into unconstrained space. This is the training data that the normalizing flow is 'effectively' seeing. (c) We evaluated those samples that were at the very right bounds of the marginal distribution under the current posterior (blue) as well as under the posterior from approximately 5 rounds before (orange). The samples have consistently lower log-probability under the previous posterior, which shows that the location of the leaking mass is moving.
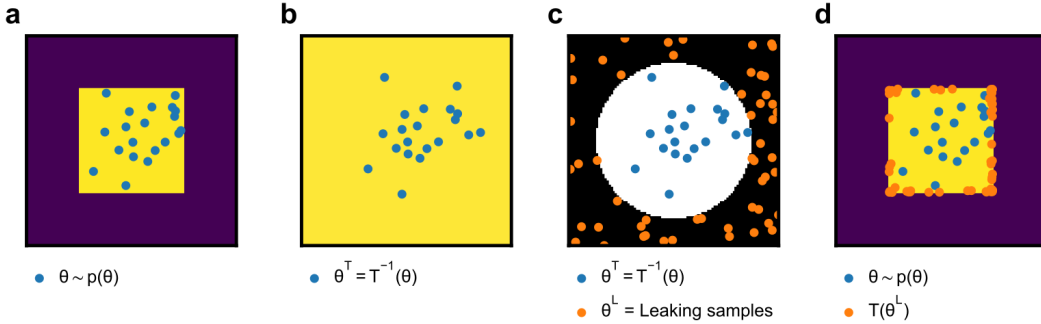
Figure 17: **Illustration of 'leakage' when prior is transformed to unconstrained space.** Note that these results are not based on an actual run of APT, but are purely for illustrative purposes. (a) The prior is a two-dimensional distribution on a constrained space (yellow region). Samples from the prior are in blue. (b) When the prior is transformed with an inverse sigmoid, its support becomes unconstrained. (c) APT will fit the posterior within the region of the training data (white region, blue samples). Outside of the training data, the trained density estimator can put arbitrary mass without affecting the loss (black region). Samples from this region are in orange. (d) When these 'leaking' samples (obtained with APT) are transformed back into constrained space, the 'leaking' mass ends up on the bounds of the prior.
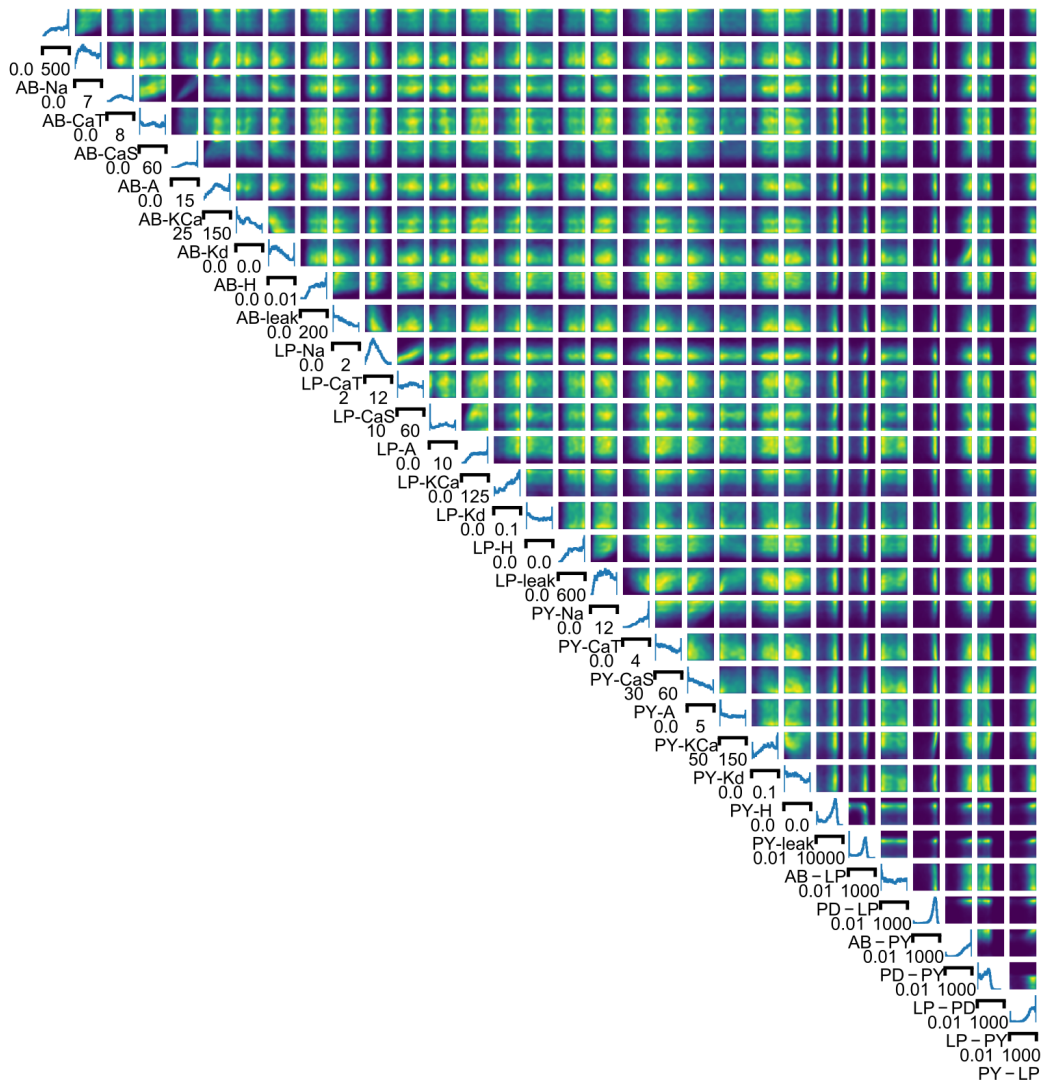
30

Figure 18: **Posterior distribution inferred by APT for the pyloric network model.**
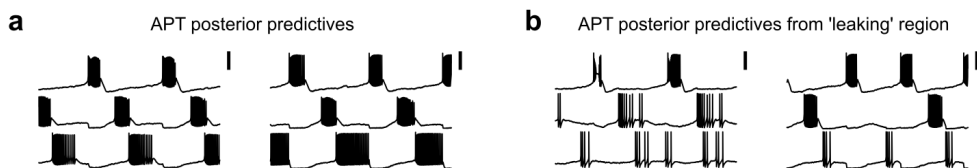

Figure 19: **Failure of APT when transformed to constrained space.** (a) Activity generated by two parameter sets sampled from the posterior distribution obtained with APT. We ensured that the shown parameter sets are not sampled from the very bounds of posterior distribution (i.e., that they were not sampled from the peak shown in Fig. 5c). (b) Activity generated by two parameter sets sampled from the posterior distribution obtained with APT. We specifically selected parameter sets whose value of $\overline{g}_{KCa}$ in the AB-PD neuron was above 14.999 (i.e., those samples which are in the peak shown in Fig. 5c).
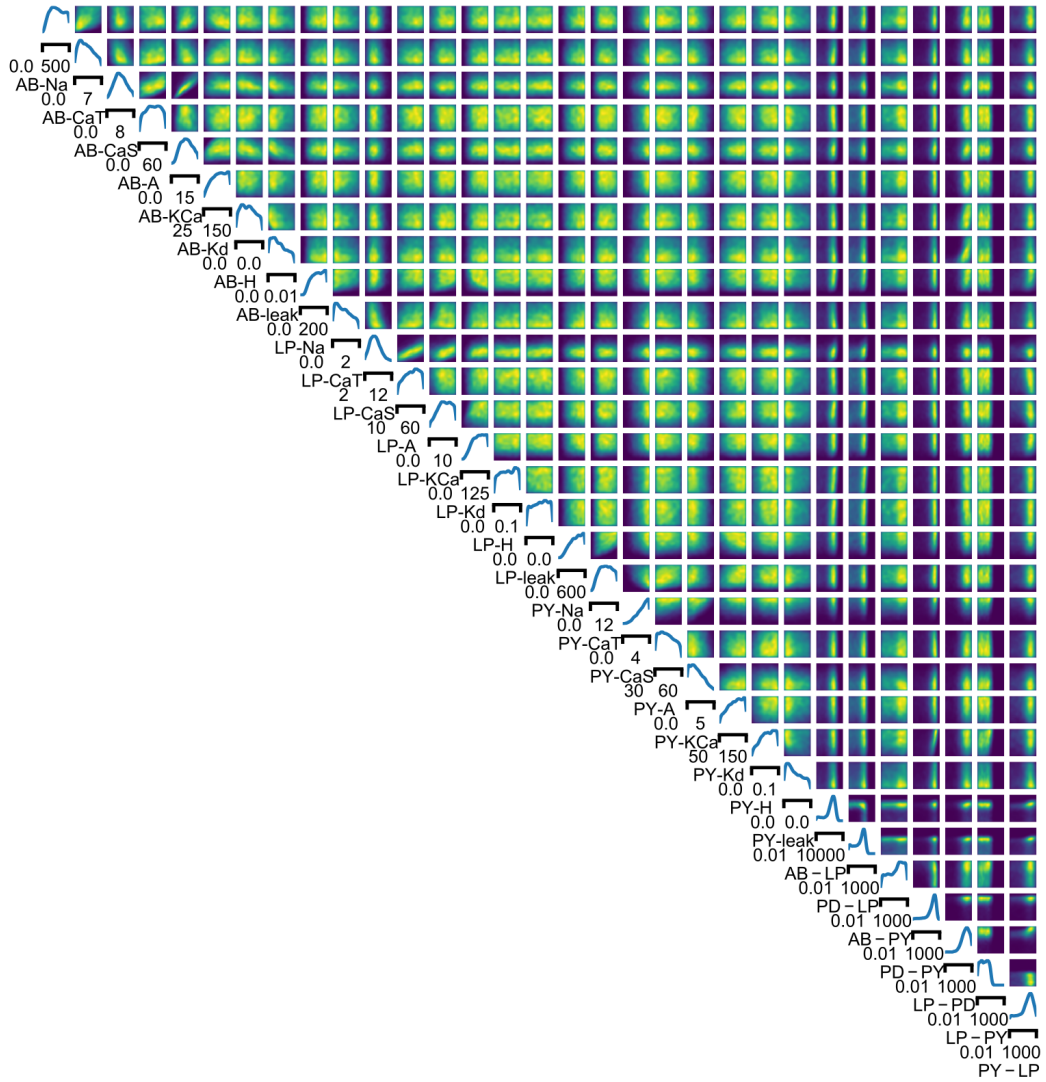
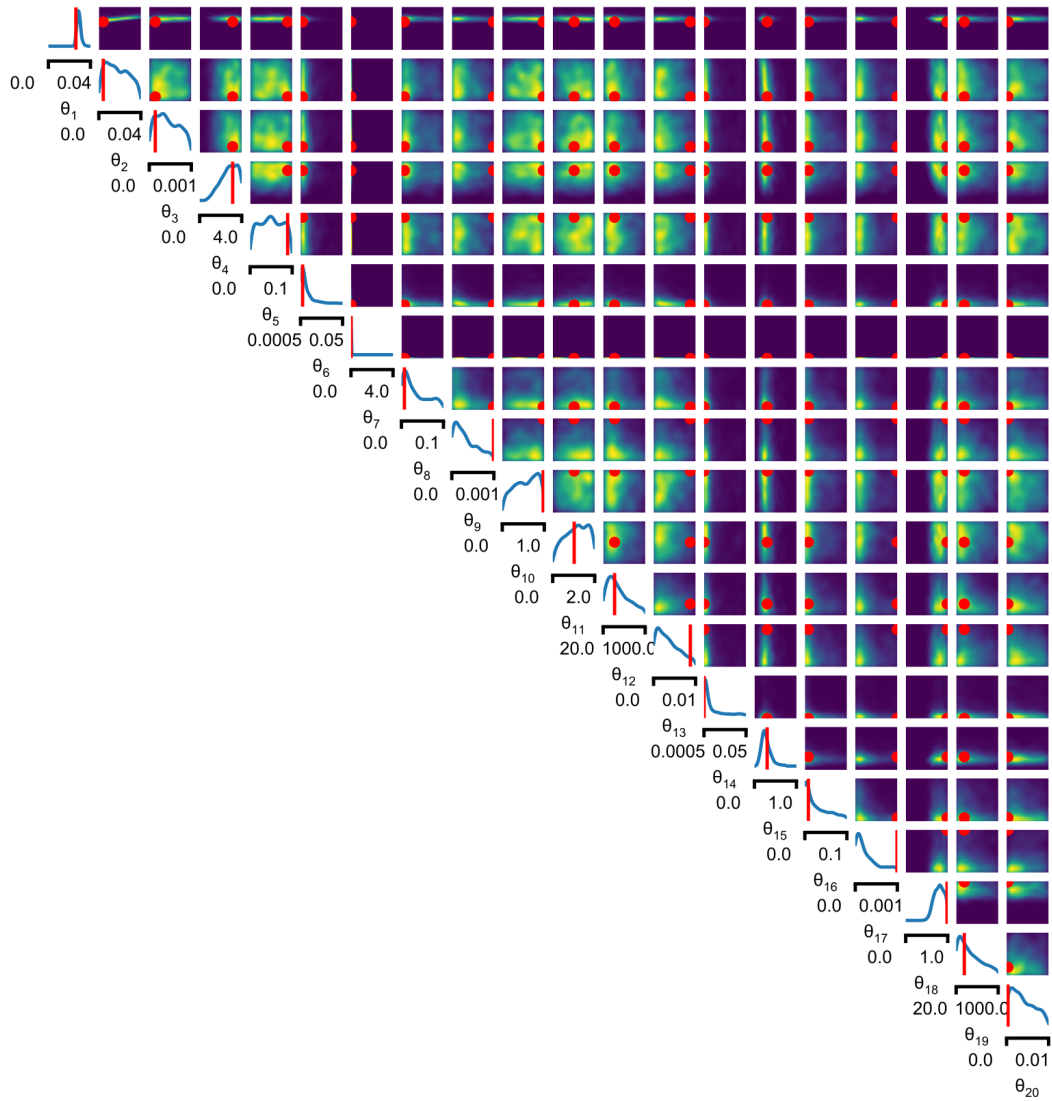Figure 20: **Posterior distribution inferred by TSNPE for the pyloric network model.**

Figure 21: **Full posterior distribution over biophysical parameters for the layer 5 pyramidal cell.** Parameter names can be found in Appendix Sec. 6.14. Red dots are the ground-truth parameters.
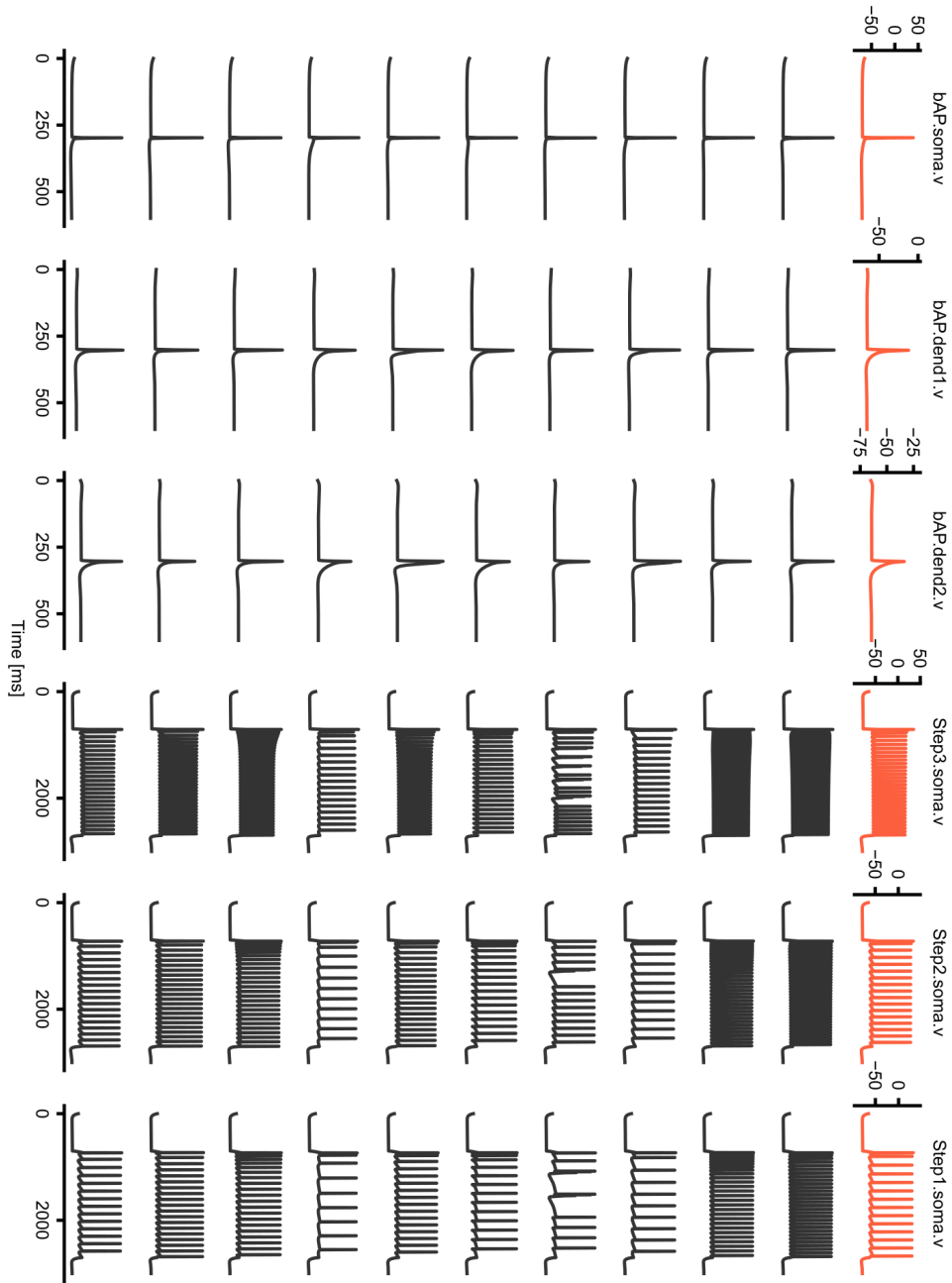
Figure 22: **Observed data (orange, top row) and ten posterior predictives obtained with TSNPE (black).**
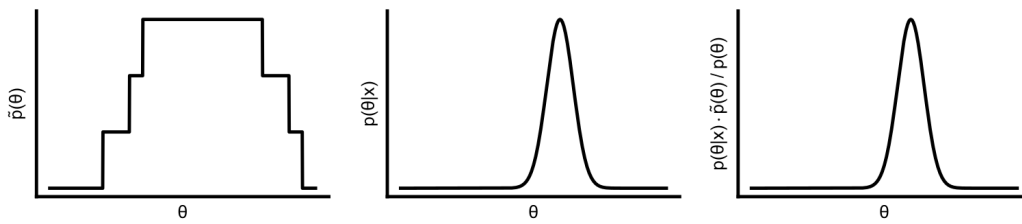
Figure 23: **Truncated proposals when pooling data from multiple rounds.** Assume a uniform prior. Left: Proposal that is the average of the proposal over three rounds. Middle: true posterior. Right: the approximate posterior converges to $p(\boldsymbol{\theta}|\mathbf{x}_o)\frac{\tilde{p}(\boldsymbol{\theta})}{p(\boldsymbol{\theta})}$ [Papamakarios and Murray, 2016, Lueckmann et al., 2017, Greenberg et al., 2019]. This matches the true posterior even though the proposal is not constant *outside* of the HPR$_\epsilon$ of the true posterior.